Lipid disequilibrium disrupts ER proteostasis by impairing ERAD substrate glycan trimming and dislocation

Milton To[a,†], Clark W. H. Peterson[a,†], Melissa A. Roberts[a], Jessica L. Counihan[a,b,c], Tiffany T. Wu[a], Mercedes S. Forster[a], Daniel K. Nomura[a,b,c], and James A. Olzmann[a,*]

[a]Department of Nutritional Sciences and Toxicology, [b]Department of Chemistry, and [c]Department of Molecular and Cell Biology, University of California, Berkeley, Berkeley, CA 94720

ABSTRACT **The endoplasmic reticulum (ER) mediates the folding, maturation, and deployment of the secretory proteome. Proteins that fail to achieve their native conformation are retained in the ER and targeted for clearance by ER-associated degradation (ERAD), a sophisticated process that mediates the ubiquitin-dependent delivery of substrates to the 26S proteasome for proteolysis. Recent findings indicate that inhibition of long-chain acyl-CoA synthetases with triacsin C, a fatty acid analogue, impairs lipid droplet (LD) biogenesis and ERAD, suggesting a role for LDs in ERAD. However, whether LDs are involved in the ERAD process remains an outstanding question. Using chemical and genetic approaches to disrupt diacylglycerol acyltransferase (DGAT)–dependent LD biogenesis, we provide evidence that LDs are dispensable for ERAD in mammalian cells. Instead, our results suggest that triacsin C causes global alterations in the cellular lipid landscape that disrupt ER proteostasis by interfering with the glycan trimming and dislocation steps of ERAD. Prolonged triacsin C treatment activates both the IRE1 and PERK branches of the unfolded protein response and ultimately leads to IRE1-dependent cell death. These findings identify an intimate relationship between fatty acid metabolism and ER proteostasis that influences cell viability.**

Monitoring Editor
Reid Gilmore
University of Massachusetts

Received: Jul 5, 2016
Revised: Nov 9, 2016
Accepted: Nov 15, 2016

INTRODUCTION

As the entry point into the secretory pathway, the endoplasmic reticulum (ER) is host to an extensive cohort of enzymes and chaperones that coordinate the folding, modification, and deployment of a large fraction of the proteome. Failure of secretory proteins to achieve their native structure due to mutations, errors in transcription or translation, protein damage, or inefficient folding can have dire consequences for cellular physiology and has been implicated in the etiology of numerous human diseases (Guerriero and Brodsky, 2012). Incorrect protein folding not only can result in a reduction in protein activity (i.e., loss of function), but it can also lead to the generation of cytotoxic protein aggregates (i.e., gain of function). To ensure the fidelity of the secretory proteome, the ER has evolved a quality control system that detects terminally misfolded and unoligomerized proteins and targets them for clearance via a process known as ER-associated degradation (ERAD; Olzmann *et al.*, 2013a; Christianson and Ye, 2014; Stevenson *et al.*, 2016). The cell also responds to perturbations in ER homeostasis by activating the unfolded protein response (UPR; Walter and Ron, 2011; Wang and Kaufman, 2016), a set of signaling pathways that enhance the overall folding capacity of the ER.

ERAD involves a series of spatially and temporally coupled steps that mediate substrate recognition, dislocation (also known as retrotranslocation) across the ER membrane into the cytoplasm, ubiquitination, and targeting to the proteasome for proteolysis (Olzmann *et al.*, 2013a; Christianson and Ye, 2014; Stevenson *et al.*, 2016).

This article was published online ahead of print in MBoC in Press (http://www.molbiolcell.org/cgi/doi/10.1091/mbc.E16-07-0483) on November 23, 2016.

†These authors contributed equally.

*Address correspondence to: James A. Olzmann (olzmann@berkeley.edu).

Abbreviations used: AC, acylcarnitine; CG, core glycosylated; CHOP, C/EBP homologous protein; DAG, diacylglycerol; DD, destabilized domain; DGAT, diacylglycerol acyltransferase; ER, endoplasmic reticulum; ERAD, endoplasmic reticulum–associated degradation; GFP, green fluorescent protein; IRE1, inositol-requiring enzyme-1; LD, lipid droplet; Mat., mature; MEF, mouse embryonic fibroblast; NHK, null Hong Kong; PERK, protein kinase RNA (PKR)–like ER kinase; PNGase F, peptide-*N*-glycosidase F; SRM, single-reaction monitoring; TAG, triacylglycerol; TTR, transthyretin; UPR, unfolded protein response.

Although the mechanism by which substrates are triaged for degradation is incompletely understood, it is clear that the structure of substrate-conjugated N-linked glycans provides a "molecular code" that plays a determining role in the fate of secretory proteins (Xu and Ng, 2015). During insertion into the ER, the majority of the secretory proteome is modified by covalent attachment of a triantennary glycan moiety (Cherepanova *et al.*, 2016). Progressive trimming by ER-resident mannosidases exposes an α-1,6–linked mannose, which acts as a signal for ERAD and is recognized by the mannose 6-phosphate receptor homology (MRH) domain of the ER lectin, OS-9, and possibly a second ER lectin, XTP3-B (Satoh *et al.*, 2010). These two ER lectins interact with the Hrd1 luminal adaptor SEL1L (Christianson *et al.*, 2008; Mueller *et al.*, 2008; Tyler *et al.*, 2012), facilitating substrate delivery for dislocation. Most models posit that the AAA ATPase VCP (also known as p97) then extracts substrates from proteinaceous pores in the membrane, possibly formed by the E3 ubiquitin ligase Hrd1 (Carvalho *et al.*, 2010; Stein *et al.*, 2014; Baldridge and Rapoport, 2016), the derlin family of proteins (Lilley and Ploegh, 2004; Ye *et al.*, 2004; Greenblatt *et al.*, 2011; Mehnert *et al.*, 2014), or, in some cases, the Sec 61 translocon (Plemper *et al.*, 1997; Scott and Schekman, 2008).

In addition to its role as a protein-folding compartment, the ER functions as a major site of lipid metabolism, mediating the synthesis of important lipids (e.g., phospholipids, sterols, and neutral lipids) and the biogenesis of lipid storage organelles called lipid droplets (LDs; Walther and Farese, 2012; Pol *et al.*, 2014; Hashemi and Goodman, 2015). LDs are ubiquitous, conserved organelles composed of a neutral lipid core (e.g., triacylglycerol [TAG] and sterol esters) encircled by a phospholipid monolayer. Whereas the hydrophobic core of LDs is devoid of proteins, the bounding phospholipid monolayer is decorated with a unique proteome that regulates LD growth, breakdown, and trafficking. LDs function as dynamic repositories of lipids, protecting the cell from fatty acid–induced toxicity (Listenberger *et al.*, 2003) and providing the cell with an "on-demand" source of lipids for membrane biogenesis (Kurat *et al.*, 2009), energy production via β-oxidation (Rambold *et al.*, 2015), and use as ligands in lipid signaling pathways (Haemmerle *et al.*, 2011; Tang *et al.*, 2013). Several unexpected roles have also been identified for LDs, such as the regulation of the hepatitis C life cycle (Miyanari *et al.*, 2007; Herker *et al.*, 2010), the sequestration of histones (Cermelli *et al.*, 2006; Anand *et al.*, 2012), and the control of cytosolic inclusion body clearance (Moldavski *et al.*, 2015).

Reports have identified a number of intriguing links between ERAD and LDs. A subset of proteins implicated in ERAD, including UBXD8, UBXD2, VCP, AUP1, and Ube2g2, were identified in proteomic analyses of buoyant, LD-enriched biochemical fractions (Brasaemle *et al.*, 2004; Liu *et al.*, 2004; Hodges and Wu, 2010), and the localization of these proteins to the LD surface was confirmed by fluorescence microscopy (Mueller *et al.*, 2008; Zehmer *et al.*, 2009; Klemm *et al.*, 2011; Spandl *et al.*, 2011; Suzuki *et al.*, 2012; Jo *et al.*, 2013; Olzmann *et al.*, 2013b). This subset of ERAD factors has been implicated in the regulation of LD abundance, size, and clustering (Mueller *et al.*, 2008; Zehmer *et al.*, 2009; Klemm *et al.*, 2011; Spandl *et al.*, 2011; Suzuki *et al.*, 2012; Jo *et al.*, 2013; Olzmann *et al.*, 2013b), but whether these effects on LDs are related to their functions in ERAD remains to be determined. ERAD substrates have also been observed on the LD surface (e.g., ApoB100 [Ohsaki *et al.*, 2006; Suzuki *et al.*, 2012]) and in ER subdomains that are closely juxtaposed to LDs (e.g., 3-hydroxy-3-methylglutaryl-coenzyme A reductase [HMGCR; Hartman *et al.*, 2010]). In addition, ER stress induces LD biogenesis (Fei *et al.*, 2009; Vevea *et al.*, 2015), and loss of LDs activates the UPR (Garbarino *et al.*, 2009; Petschnigg *et al.*, 2009; Olzmann and Kopito, 2011; Velázquez *et al.*, 2016).

Indirect experimental evidence supporting a functional role for LDs in ERAD came from studies employing triacsin C, a polyunsaturated fatty acid analogue that inhibits long-chain acyl-CoA synthetases (ACSLs; Tomoda *et al.*, 1987; Igal *et al.*, 1997) and blocks LD biogenesis (Fujimoto *et al.*, 2007; Kassan *et al.*, 2013). These studies found that triacsin C impaired the degradation kinetics of several ERAD substrates, including the null Hong Kong (NHK) mutant of α-1 antitrypsin (Klemm *et al.*, 2011), a truncated variant of ribophorin I (Klemm *et al.*, 2011), class I MHC heavy chain (Klemm *et al.*, 2011), and HMGCR (Hartman *et al.*, 2010; Jo *et al.*, 2013). Together these findings led to multiple models of how LDs might be involved in ERAD (Ploegh, 2007; Hartman *et al.*, 2010; Klemm *et al.*, 2011; Suzuki *et al.*, 2012; Jo *et al.*, 2013; Vevea *et al.*, 2015): 1) LD biogenesis is coupled to the dislocation of luminal ERAD substrates via the formation of transient pores in the membrane or the dislocation of integral membrane ERAD substrates via capture in the membrane of an exiting LD, 2) ERAD substrate dislocation and ubiquitination preferentially occur in LD-associated ER subdomains, and/or 3) ERAD substrates are sequestered on the surface of LDs as an intermediate step en route to the proteasome. Although these models are attractive, triacsin C is not a specific inhibitor of LD biogenesis, as it also affects unrelated processes that require activated fatty acids (e.g., de novo phospholipid synthesis; Igal *et al.*, 1997). Moreover, the degradation kinetics of several ERAD substrates was unaffected in a strain of yeast lacking LDs (Olzmann and Kopito, 2011; Nakatsukasa and Kamura, 2016), indicating either that LD formation is not essential for ERAD or that there are unrecognized differences between the ERAD process in yeast and mammalian cells. Thus, the functional relationship between ERAD and LDs remains unresolved.

In this study, we focused our attention on the effect of triacsin C on ERAD and the potential requirement of LDs for ERAD in mammalian cells. Our results demonstrate that, as in yeast (Olzmann and Kopito, 2011; Nakatsukasa and Kamura, 2016), LDs are dispensable for ERAD in mammalian cells. However, our data indicate that triacsin C causes widespread changes in the cellular lipid composition, impairs ERAD substrate glycan trimming and dislocation, and induces the UPR, culminating in cell death. These findings support a fundamental connection between fatty acid metabolism and ER proteostasis.

RESULTS

Inhibition of long-chain acyl-CoA synthetases with triacsin C impairs select ERAD pathways

To examine the effect of triacsin C on ERAD, we analyzed the degradation kinetics of a panel of substrates that reflect a range of topologies and use distinct degradation pathways (Figure 1A). The panel included an endogenous ERAD substrate, CD147, which is a glycosylated type I transmembrane protein that is recognized as an unassembled subunit of an oligomeric complex and is constitutively degraded by a Hrd1/SEL1L pathway (Tyler *et al.*, 2012). We also tested two exogenously expressed mutant substrates: the NHK mutant of α-1 antitrypsin—a soluble, luminal substrate degraded by a Hrd1/SEL1L pathway (Christianson *et al.*, 2008; Hosokawa *et al.*, 2008)—and the ΔF508 mutant cystic fibrosis transmembrane conductance regulator (CFTRΔF508)—a polytopic integral membrane substrate degraded by multiple E3 ligase pathways (Meacham *et al.*, 2001; Younger *et al.*, 2006; Morito *et al.*, 2008).

To determine the kinetics of triacsin C treatment on ERAD disruption, we performed a time course of triacsin C incubation and

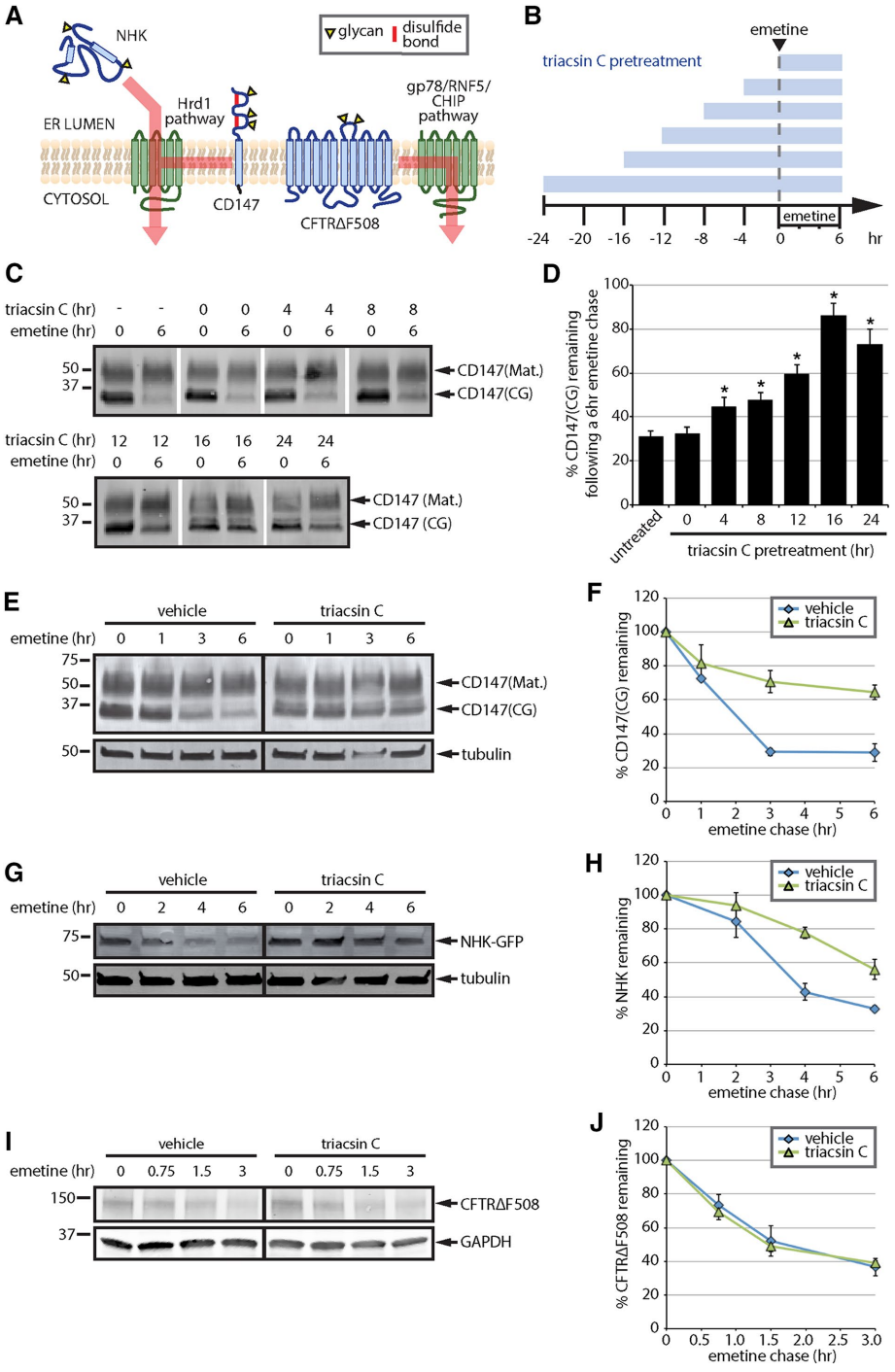

FIGURE 1: Triacsin C inhibits a subset of ERAD pathways. (A) ERAD substrate panel, indicating substrate topology and degradation pathway(s). Substrates are indicated in blue and ERAD components in green. Yellow triangles indicate N-linked glycans. (B) Triacsin C treatment time course. Triacsin C was added for the indicated times (blue bars) and maintained in the medium throughout the emetine chase. (C) HEK293 cells were pretreated with 1 μg/ml triacsin C for the indicated times (as depicted in B), followed by addition of 75 μM emetine for 6 h. CD147 levels were assessed by immunoblotting of SDS lysates. (D) The relative CD147(CG) levels in C were quantified and are presented as percentage of the levels at time 0 h ($n = 3$). Asterisk indicates significant stabilization ($p < 0.05$). (E) HEK293 cells were pretreated with vehicle or 1 μg/ml triacsin C for 16 h, followed by 75 μM emetine for the indicated times. CD147 levels were assessed by immunoblotting of SDS lysates. (F) The relative levels of CD147(CG) in E were quantified and are presented as percentage of the levels at time 0 h ($n = 3$). (G) HEK293 cells expressing NHK-GFP were pretreated with vehicle or 1 μg/ml triacsin C for 16 h, followed by 75 μM emetine for the indicated times. NHK-GFP levels were assessed by immunoblotting of SDS lysates. (H) The relative levels of NHK-GFP in G were quantified and are presented as percentage of the levels at time 0 h ($n = 3$). (I) HEK293 cells expressing CFTRΔF508 were pretreated with vehicle or 1 μg/ml triacsin C for 16 h, followed by 75 μM emetine for the indicated times. CFTRΔF508 levels were assessed by immunoblotting of SDS lysates. (J) The relative levels of CFTRΔF508 in I were quantified and are presented as percentage of the levels at time 0 h ($n = 4$). Mat., mature; CG, core glycosylated. Error bars indicate SEM.

analyzed the degradation of CD147 during emetine translation shutoff (Figure 1, B–D). As expected (Tang, 2004; Tyler *et al.*, 2012), CD147 migrated as two primary species: a high–molecular weight plasma membrane form bearing complex glycans (CD147(mature [Mat.])) and a lower–molecular weight ER form bearing the core-glycan structure (CD147(CG); Figure 1C). CD147(CG) was degraded during the 6-h emetine chase (Figure 1, C and D). Addition of triacsin C at time 0 of the emetine chase had no effect on CD147(CG) degradation (Figure 1, C and D). Increasing stabilization of CD147(CG) was observed as the triacsin C preincubation time was lengthened, with a maximal stabilization occurring after a 16-h triacsin C pretreatment (Figure 1, C and D). Using the 16-h triacsin C pretreatment, we analyzed the degradation kinetics of our full panel of ERAD substrates (Figure 1, E–J). The Hrd1 substrate CD147(CG) was stabilized by triacsin C pretreatment (Figure 1, E and F). Although the majority of newly synthesized CD147 is degraded by ERAD, a small fraction can correctly assemble and mature by trafficking through the Golgi to the plasma membrane (Tang, 2004; Tyler *et al.*, 2012). To account for both fates of CD147, we performed radioactive pulse-chase experiments (Supplemental Figure S1A). Over the 6-h time course of our experiment, no CD147 maturation was detected, and triacsin C pretreatment stabilized CD147(CG). These results indicate that the effect of triacsin C is due to impairment of CD147 degradation rather than maturation. The Hrd1 luminal substrate NHK–green fluorescent protein (GFP) was also stabilized by triacsin C pretreatment (Figure 1, G and H). No secretion of NHK-GFP was observed in this cell line (Supplemental Figure S1B). In contrast to CD147 and NHK-GFP, CFTRΔF508 degradation kinetics was unaffected by the triacsin C pretreatment (Figure 1, I and J). These data demonstrate that treatment with the ACSL inhibitor triacsin C impairs select ERAD pathways.

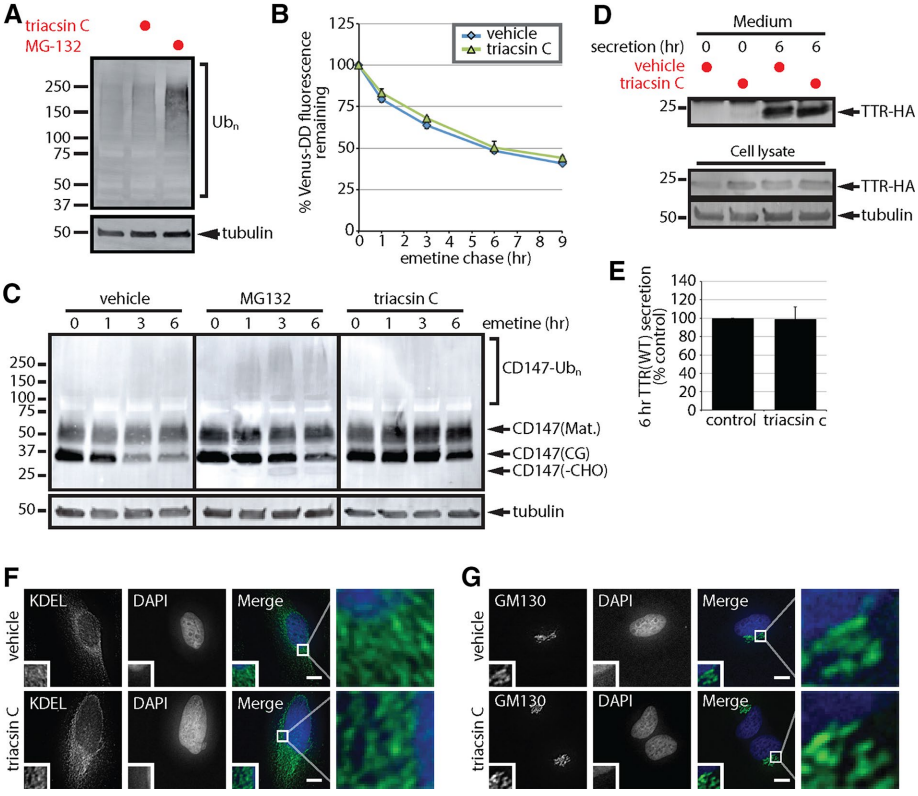

FIGURE 2: Triacsin C does not generally inhibit the ubiquitin-proteasome system or protein secretion. (A) SDS lysates from HEK293 cells incubated with 1 µg/ml triacsin C for 16 h or 10 µM MG-132 for 6 h were analyzed by immunoblotting. (B) U2OS cells stably expressing Venus-DD were incubated with vehicle or 1 µg/ml triacsin C for 16 h, followed by emetine treatments for the indicated times. Venus fluorescence levels were monitored by flow cytometry and quantified as the percentage of the levels at time 0 h ($n = 3$). (C) HEK293 cells were incubated with vehicle or 1 µg/ml triacsin C for 16 h and then treated with 75 µM emetine for the indicated times. Where indicated, 10 µM MG-132 was added at the beginning of the emetine chase. The levels of the different forms of CD147 were assessed by immunoblotting of SDS lysates. (D) HEK293 cells expressing TTR-HA were treated with vehicle or 1 µg/ml triacsin C for 16 h. Cells were washed with PBS, and the medium was replaced with serum-free OPTI-MEM containing vehicle or 1 µg/ml triacsin C for the remaining 6 h. Lysates and TTR-HA immunoprecipitated from the media were analyzed by immunoblotting. (E) The levels of TTR-HA in the media were quantified from D and are presented as percentage of the levels in the control sample ($n = 3$). (F, G) The morphology of the ER, anti-KDEL (green) and the Golgi complex, anti-GM130 (green), in HeLa cells treated with vehicle or 1 µg/ml triacsin C for 16 h was analyzed by immunofluorescence microscopy. Nuclei were stained with DAPI (blue). Scale bar, 10 µm. Mat., mature; CG, core glycosylated; -CHO, deglycosylated. Error bars indicate SEM.

Triacsin C does not generally inhibit the ubiquitin-proteasome system

Our finding that triacsin C inhibits the degradation of a subset of ERAD substrates suggests that triacsin C treatment does not generally inhibit the ubiquitin-proteasome system (UPS). In agreement with this notion, ubiquitinated proteins accumulated in cells treated with the proteasome inhibitor MG-132, but not with triacsin C (Figure 2A). To assess more directly the effect of triacsin C on the degradation of cytosolic proteins, we used flow cytometry to measure the degradation kinetics of a cytosolic UPS reporter (Figure 2B). This reporter consists of the Venus fluorescent protein fused to a destabilized domain (Venus-DD), a variant FK506-binding domain from FKBP12 that, in the absence of the small molecule shield-1, is misfolded and rapidly degraded via the UPS (Banaszynski *et al.*, 2006; Egeler *et al.*, 2011; Bersuker *et al.*, 2016). Triacsin C had no significant effect on the constitutive degradation of Venus-DD (Figure 2B), indicating that triacsin C does not generally affect the degradation of cytosolic UPS substrates.

After dislocation, ERAD substrates are deglycosylated by the cytosolic peptide:*N*-glycanase (PNGase) and cleared by the UPS (Olzmann *et al.*, 2013a; Xu and Ng, 2015). Thus, the presence and accumulation of a deglycosylated form of ERAD substrates reflect inefficient coupling of dislocation with proteasomal degradation. Incubation with the proteasome inhibitor MG-132 during an emetine chase resulted in the accumulation of deglycosylated CD147 (CD147(-CHO)), indicating the buildup of cytosolically dislocated CD147 (Figure 2C). CD147 deglycosylated in vitro by incubation with the glycosidase PNGase F resolved at the same molecular weight as the CD147 band that accumulated in MG-132–treated cells, and no additional lower–molecular weight forms appeared (Supplemental Figure S2), confirming the identify of the CD147(-CHO) species. A portion of CD147 also migrated in a high–molecular weight smear, likely representing ubiquitinated CD147 (Figure 2C). In contrast to MG-132, triacsin C pretreatment solely stabilized CD147(CG); deglycosylated CD147 and ubiquitinated CD147 were absent (Figure 2C). Together, these data indicate that triacsin C impairs ERAD upstream of the proteasome and does not cause a global defect in the UPS.

Triacsin C does not impair protein secretion

Dysregulated lipid metabolism can alter organelle morphology and function (Han *et al.*, 2008; Adeyo *et al.*, 2011; Thibault *et al.*, 2012), and disruptions in ER-to-Golgi trafficking reduce the degradation of some ERAD substrates (Caldwell *et al.*, 2001; Vashist *et al.*, 2001; Taxis *et al.*, 2002). To examine the function of the secretory pathway, we analyzed the secretion of hemagglutinin-tagged transthyretin (TTR-HA), a tetrameric protein that is normally secreted into the serum, where it functions as a carrier of the thyroid hormone thyroxine. Similar levels of TTR-HA were immunoprecipitated from media isolated from cells incubated in the presence or absence of triacsin C (Figure 2, D and E), indicating that triacsin C pretreatment does not affect TTR secretion. Furthermore, the overall morphology of the ER (Figure 2F) and Golgi complex (Figure 2G) remained unperturbed by a triacsin C pretreatment at the resolution of fluorescence deconvolution microscopy. Together, these results indicate that the secretory system remains functionally and morphologically intact after a 16-h triacsin C treatment.

Triacsin C impairs CD147 glycan trimming

Our initial results indicated that triacsin C affects ERAD upstream of the proteasome (Figure 2). To determine more precisely the steps in ERAD that are compromised, we focused our attention on the degradation of the endogenous substrate CD147, which was

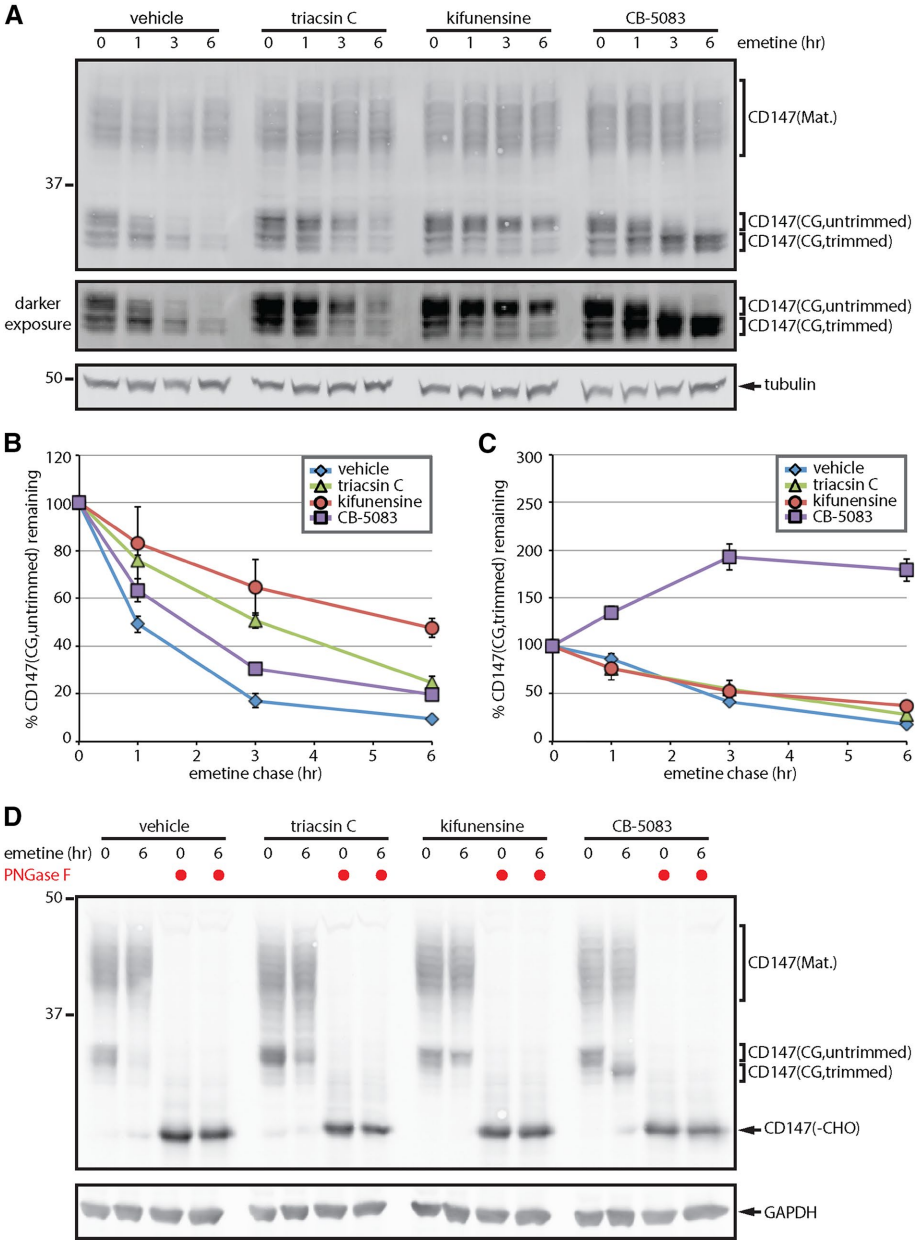

FIGURE 3: Triacsin C impairs ERAD substrate glycan trimming. (A) HEK293 cells were pretreated with vehicle or 1 μg/ml triacsin C for 16 h, followed by 75 μM emetine for the indicated times. Where indicated, 5 μg/ml kifunensine and 5 μM CB-5083 were added at the beginning of the emetine chase. SDS lysates were separated on large-format SDS–PAGE gels and analyzed by immunoblotting to visualize the different CD147 glycoforms. A darker exposure of the CD147(CG) bands is provided to facilitate visualization of the different trimmed glycoforms. (B, C) The relative levels of untrimmed CD147(CG) (B) and trimmed CD147(CG) (C) were quantified from A and are presented as percentage of the levels at time 0 h ($n = 3$). (D) Lysates from cells treated as in A were incubated with PNGase F as indicated and analyzed by immunoblotting. Mat., mature; CG, core glycosylated; -CHO, deglycosylated. Error bars indicate SEM.

strongly stabilized by triacsin C (Figure 1). Glycan trimming is often believed to be one of the most upstream events in ERAD, potentially acting as a timing mechanism that releases a substrate from futile calnexin/calreticulin folding cycles and facilitates targeting for degradation by enabling direct interactions with the ERAD-implicated lectins (Xu and Ng, 2015). The various trimmed CD147(CG) glycoforms are not resolved on small SDS–PAGE gels. Therefore, to examine a potential effect of triacsin C on CD147(CG) glycan trimming, we separated CD147 on large-format SDS–PAGE gels (Figure 3A). On these larger gels, the variety of CD147 glycoforms becomes evident, and CD147(CG) is resolved as approximately five bands (Figure 3A). Treatment of lysates in vitro with PNGase F collapsed all CD147 forms into a single band of ~29 kDa (Figure 3D), consistent with the conjecture that the variations in the CD147 banding pattern reflect the diversity of CD147 glycoforms.

During the course of an emetine translation shutoff experiment, the upper CD147(CG) bands were rapidly lost (Figure 3, A and B, vehicle), whereas the lower bands displayed a slight lag period before clearance (Figure 3, A and C, vehicle). These results are consistent with the conversion of CD147(CG) from a slower-migrating, untrimmed form into a faster-migrating, trimmed form before degradation. Treatment with the mannosidase inhibitor kifunensine (Figure 3, A–C, kifunensine) or the glucosidase inhibitor deoxynojirimycin (Supplemental Figure S3) stabilized CD147(CG) in the slower-migrating form, providing evidence that these bands represent an untrimmed form of CD147(CG). It is worth noting that CD147(CG) continued to be degraded in the presence of kifunensine (Figure 3A, kifunensine), albeit at a slower rate, indicating either that glycan trimming is not a strict requirement for CD147(CG) degradation or that kifunensine inhibition of glycan trimming is incomplete. Cotreatment with kifuensine and deoxynojirimycin did not result in additional stabilization (Supplemental Figure S3). Analysis of CD147(CG) in cells pretreated with triacsin C revealed a significantly reduced rate of CD147(CG) conversion from untrimmed to the trimmed glycoform (Figure 3, A–C, triacsin C), similar to the effect of kifunensine. In contrast, blocking CD147(CG) degradation at a downstream step with the VCP inhibitor CB-5083 resulted in the accumulation of a lower–molecular weight, presumably highly trimmed form of CD147(CG) (Figure 3, A–C, CB-5083). These data suggest that triacsin C impairment in ERAD is caused, at least in part, through inhibition of substrate glycan trimming.

Triacsin C disrupts CD147 delivery to the Hrd1 dislocation complex

CD147 is degraded via an ERAD pathway that requires Hrd1, SEL1L, and, to some extent, the lectins OS-9 and XTP3-B (Tyler *et al.*, 2012). The Hrd1 dislocation complex is a membrane-embedded, macromolecular complex (Mueller *et al.*, 2008; Christianson *et al.*, 2012). Several properties of membrane lipids can influence the interactions and functions of membrane-embedded protein complexes

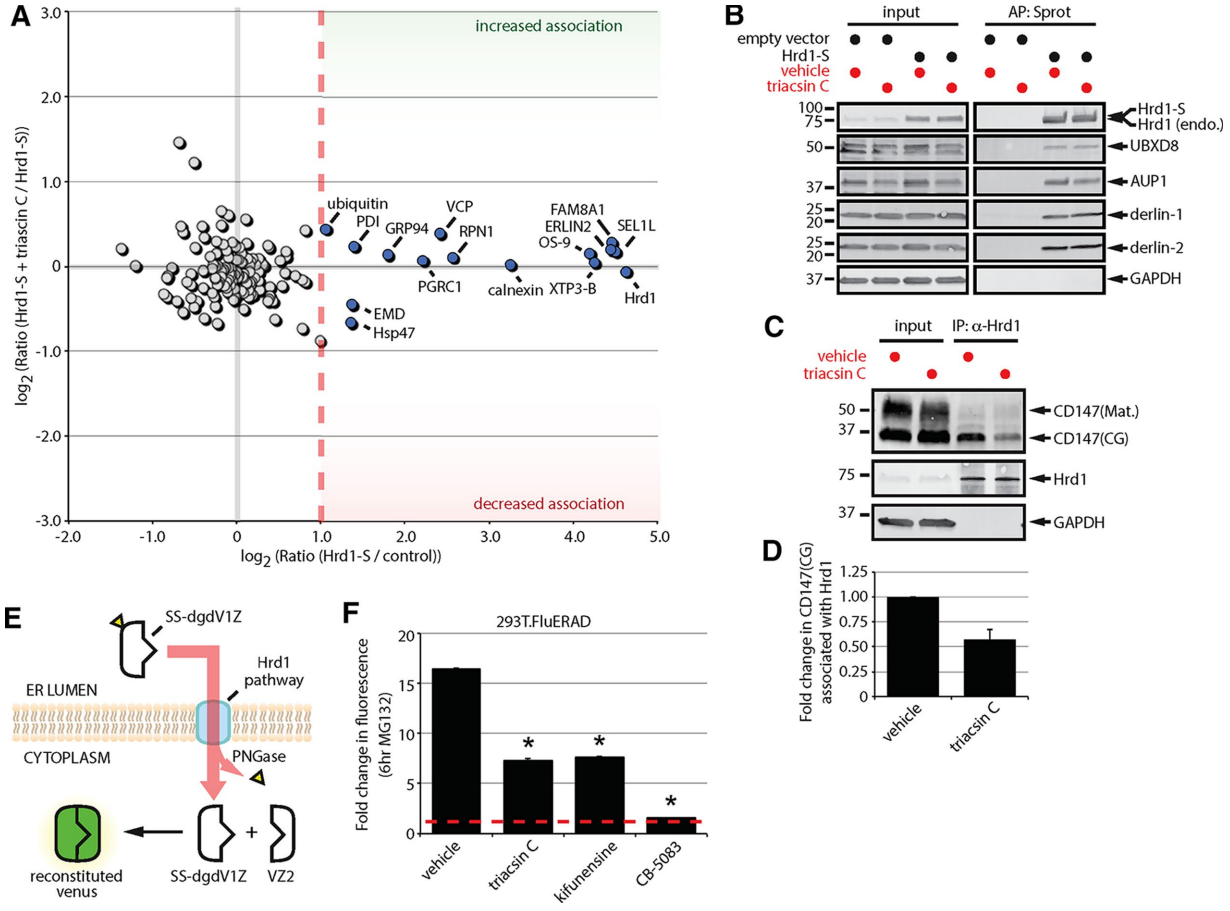

FIGURE 4: Triacsin C impairs substrate delivery to and dislocation from the Hrd1 complex. (A) Two-dimensional plot representing the proteomic analysis of Hrd1-S interactors from a triple SILAC experiment. The ratio of Hrd1-S/control on the *x*-axis indicates the strength of the interaction under basal conditions. The ratio of Hrd1-S + triacsin C/Hrd1-S on the *y*-axis indicates the change in the interaction in response to triacsin C treatment. Gray filled circles are nonspecific interactors, and blue filled circles are high-confidence interactors. (B) HEK293 cells expressing an empty vector or S-tagged Hrd1 were pretreated with vehicle or 1 μg/ml triacsin C for 16 h. Affinity-purified complexes were analyzed by immunoblotting with the indicated antibodies. (C) HEK293 cells were pretreated with vehicle or 1 μg/ml triacsin C for 16 h. Endogenous Hrd1 complexes were immunoprecipitated and analyzed by immunoblotting with the indicated antibodies. (D) The fold change in Hrd1-associated CD147(CG) in C was quantified and is presented as a bar graph ($n = 3$). (E) The split-Venus dislocation assay. See text for description. (F) 293T.FluERAD cells, which stably express the deglycosylation-dependent Venus dislocation system, were pretreated with 1 μg/ml triacsin C for 16 h, followed by a 0- or 6-h treatment with 10 μM MG-132. Where indicated, 5 μg/ml kifunensine or 5 μM CB-5083 was added together with 10 μM MG-132 for 0 or 6 h. Venus fluorescence levels were quantified by flow cytometry and are represented as the fold change relative to the 0 h. Asterisk indicates a significant decrease in the fold change in fluorescence levels ($p < 0.05$). AP, affinity purification; CG, core glycosylated; endo., endogenous; IP, immunoprecipitation; Mat., mature; Sprot, S-protein agarose. Error bars indicate SEM.

(Bogdanov *et al.*, 2008; Contreras *et al.*, 2011). To determine whether ACSL inhibition affects the composition of the Hrd1 dislocation complex, we used a quantitative triple stable isotope labeling with amino acids in cell culture (SILAC) strategy to measure the dynamics of Hrd1 interactions in response to triacsin C treatment (Figure 4A and Supplemental Tables S1 and S2). The results from this experiment are displayed in a two-dimensional plot (Figure 4A), which groups nonspecific background, as well as constitutive and dynamic interactors. Of the 145 proteins detected, 15 passed our criteria for high-confidence interactors (SILAC ratio M:L > 2-fold). In addition to the identification of Hrd1 itself (the bait), the strongest interactors (SILAC ratio M:L > 20-fold) were known members of the Hrd1 complex—SEL1L, FAM8A1, ERLIN2, OS-9, and XTP3-B. Other noteworthy interactors that were captured included proteins involved in protein folding and degradation, such as VCP, PDI, GRP94, Hsp47, calnexin, and ubiquitin. The significance of Hrd1 association with RPN1 (also known as ribophorin I), PGRC1, and EMD is unknown. These proteins are not known to be involved in protein quality control and may represent endogenous substrates of the Hrd1 complex. Several previously reported Hrd1 complex members (UBXD8, AUP1, derlin-1, derlin-2) were not detected in our SILAC experiment, possibly due to their lower abundance. Therefore, we examined the association of these interactors with Hrd1 by immunoblotting of affinity purified S-tagged Hrd1 complexes (Figure 4B). Analysis of the results from both the SILAC (Figure 4A) and immunoblotting (Figure 4B) experiments indicate that few Hrd1 interactions were affected by triacsin C treatment. The core Hrd1 complex, characterized by SEL1L, FAM8A1, XTP3-B, OS-9, and ERLIN2, remained intact after triacsin C treatment. There were minor trends toward increased associations with VCP and ubiquitin, as well as decreased association with Hsp47.

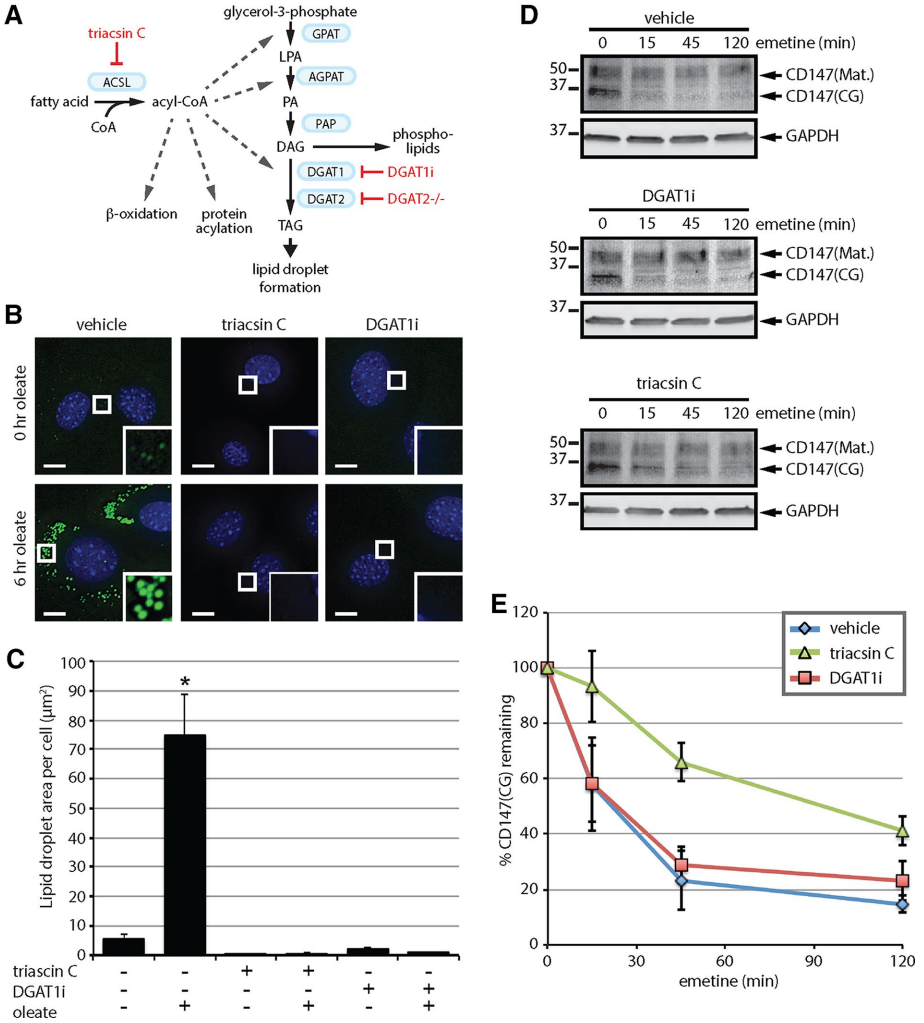

FIGURE 5: Lipid droplet biogenesis is dispensable for CD147 ERAD. (A) The Kennedy pathway of TAG synthesis indicating the enzymes (blue boxes) and metabolites. Select additional pathways that use acyl-CoA are also depicted. Approaches to disrupt LD biogenesis through the inhibition of ACSLs (triacsin C) or the DGAT enzymes (DGAT1i and DGAT2-/-) are indicated in red. (B) DGAT2-/- MEFs were pretreated with 1 μg/ml triacsin C or 20 μM DGAT1i for 3 h and then incubated with 200 μM oleate for 0 or 6 h as indicated. Fluorescence microscopy was employed to visualize LDs (green) and nuclei (blue). Scale bar, 5 μm. (C) The abundance of LDs was quantified from cells treated as shown in B. Asterisk indicates a significant increase in LD amount relative to untreated cells ($p < 0.05$). (D) DGAT2-/- MEFs were pretreated with vehicle, 1 μg/ml triacsin C, or 20 μM DGAT1i for 16 h, followed by 75 μM emetine for the indicated times. CD147 levels were assessed by immunoblotting of SDS lysates. (E) The relative levels of CD147(CG) in D were quantified and are presented as percentage of the levels at time 0 h ($n = 3$). ACSL, long-chain acyl-CoA synthetase; AGPAT, acylglycerolphosphate acyltransferase; DAG, diacylglycerol; DGAT, diacylglycerol acyltransferase; GPAT, glycerol-phosphate acyltransferase; LPA, lysophosphatidic acid; PA, phosphatidic acid; PAP, phosphatidic acid phosphatase; TAG, triacylglycerol. Error bars indicate SEM.

To examine a potential effect of triacsin C on the delivery of CD147 to the Hrd1 complex, we analyzed endogenous Hrd1 complexes immunoprecipitated from vehicle- and triacsin C–treated cells. Hrd1 bound only the ER-localized core glycosylated form of CD147 (Figure 4, C and D), supporting the specificity of the interaction with CD147. Of interest, triacsin C treatment caused a pronounced decrease in the amount of CD147(CG) that coprecipitated with Hrd1 (Figure 4, C and D). Thus, our results indicate that whereas the overall composition of the Hrd1 dislocation complex is mostly unaffected, triacsin C treatment reduces the delivery of the substrate CD147 to the Hrd1 complex.

Triacsin C impairs the dislocation of a luminal glycosylated ERAD substrate

Given the effects of triacsin C on CD147 glycan trimming (Figure 3) and association with Hrd1 (Figure 4, C and D), we predicted that triacsin C would affect substrate dislocation. The accumulation of deglycosylated CD147 in response to MG-132 treatment provides one potential method to assess dislocation. However, MG-132 also stabilized CD147(CG), and the appearance of deglycosylated CD147 was minimal and difficult to detect (Figure 2C). Therefore, to assess quantitatively the effects of triacsin C on dislocation, we used a more sensitive and robust fluorescent ERAD dislocation assay based on the reconstitution of split Venus (Figure 4E; Grotzke *et al.*, 2013). In this assay, the N-terminal half of deglycosylation-dependent Venus is fused to the H2-K^b signal sequence (SS-dgdV1Z), targeting it to the ER lumen (Grotzke *et al.*, 2013). SS-dgdV1Z is glycosylated, recognized as an aberrant protein, and dislocated into the cytosol for degradation (Grotzke *et al.*, 2013). In the presence of MG-132, SS-dgdV1Z accumulates in the cytosol and associates with the C-terminal half of Venus (VZ2), reconstituting the mature fluorescent protein and enabling dislocation to be measured by flow cytometry (Grotzke *et al.*, 2013). Of importance, the fluorescence is deglycosylation dependent (Grotzke *et al.*, 2013), ensuring that any fluorescence detected results from the dislocation of dgdV1Z from the ER lumen into the cytosol.

Incubation of 293T.FluERAD cells stably expressing SS-dgdV1Z and VZ2 with MG-132 resulted in a large increase in Venus fluorescence (Figure 4F, 16.4-fold increase). In agreement with a role for VCP in SS-dgdV1Z dislocation (Grotzke *et al.*, 2013), coincubation with CB-5083 and MG-132 nearly completely blocked the increase in fluorescence (Figure 4F, 1.6-fold increase). Similar to the effect of kifunensine treatment (Figure 4F, 7.6-fold), triacsin C treatment partially blocked the increase in fluorescence in response to MG-132 (Figure 4F, 7.3-fold). Thus, triacsin C significantly reduces the dislocation of a luminal glycosylated ERAD substrate.

Lipid droplets are dispensable for CD147 ERAD

The observation that triacsin C inhibits ERAD (Hartman *et al.*, 2010; Klemm *et al.*, 2011; Jo *et al.*, 2013; Figure 1) is in agreement with a role for LDs in ERAD; however, triacsin C is not a selective inhibitor of LD biogenesis (Figure 5A). Although a selective inhibitor of LD biogenesis has not been identified, ablation of the diacylglycerol acyltransferase (DGAT) enzymes (DGAT1 and DGAT2), which catalyze the final and committed step in TAG synthesis

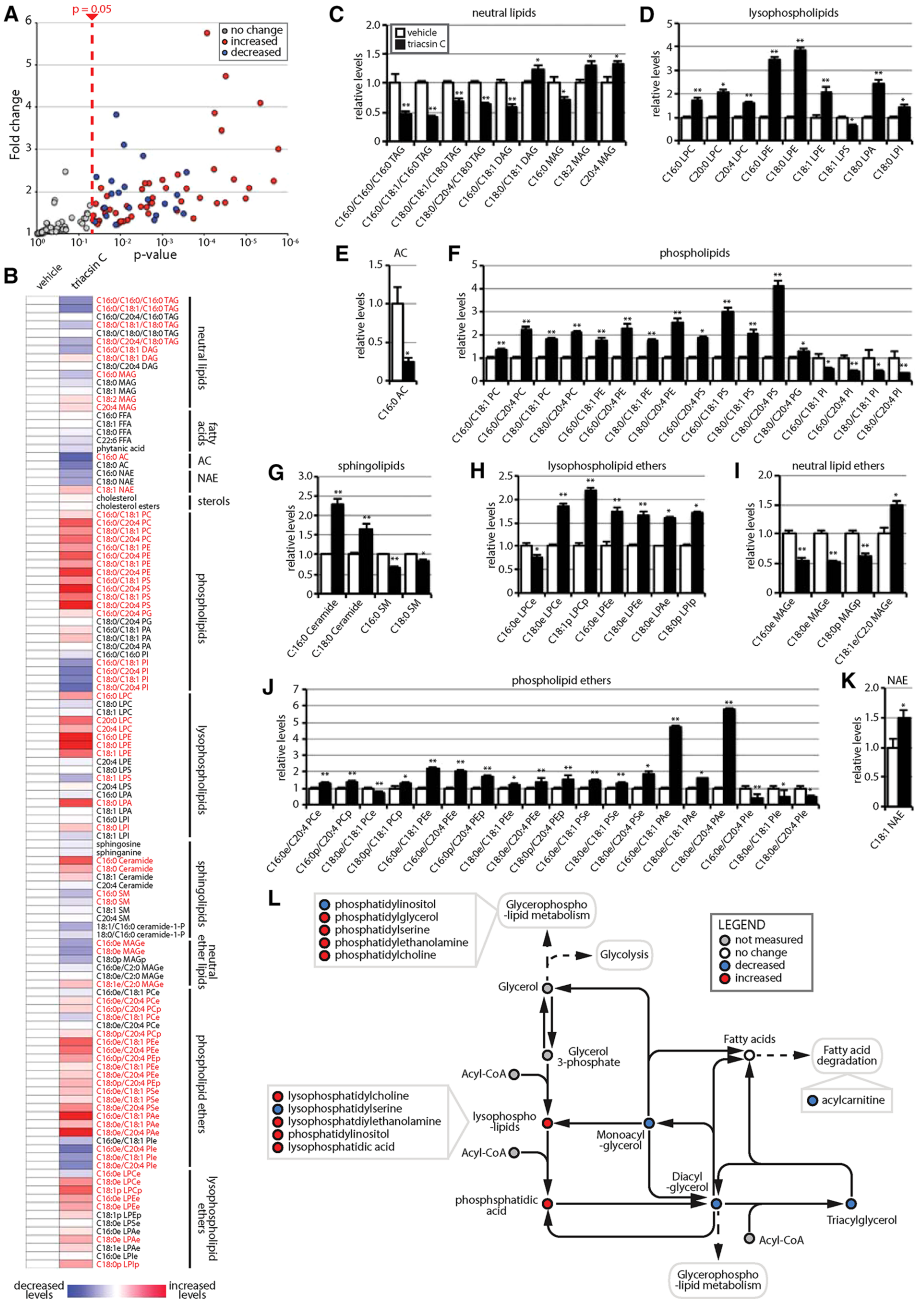

FIGURE 6: Triacsin C alters the cellular lipid landscape. Targeted metabolomic analysis of the nonpolar metabolome of cells treated with 1 µg/ml triacsin C for 16 h revealed alterations in 71 lipid species, illustrated as a volcano plot (A) and a heat map organized by lipid class (B). Red text in B indicates a significant change ($p < 0.05$). (C–K) Quantification showing the relative levels of significantly altered lipids ($n = 4$ or 5). *$p < 0.05$, **$p < 0.01$. White bars, vehicle; black bars, triacsin C. (L) Pathway map depicting the general effects of triacsin C on neutral lipids and phospholipids. DAG, diacylglycerol; FFA, free fatty acid; MAG, monoacylglycerol; NAE, *N*-acylethanolamine; PA, phosphatidic acid; PC, phosphatidylcholine; PE phosphatidylethanolamine; PG, phosphatidylglycerol; PI, phosphatidylinositol; PS, phosphatidylserine; TAG, triacylglycerol. "L" before a lipid phospholipid designation indicates lyso-; "e" after a lipid designation indicates an ether lipid; "p" after a lipid designation designates plasmalogen. Error bars indicate SEM.

(Figure 5A), causes a complete blockade of LD biogenesis in adipocytes (Harris *et al.*, 2011). Therefore, to examine a role for LDs in ERAD, we exploited a recently developed DGAT1 inhibitor, T863 (DGAT1i) (Cao *et al.*, 2011), and mouse embryonic fibroblast (MEF) cell lines lacking DGAT2 (DGAT2-/-; Stone *et al.*, 2004; Harris *et al.*, 2011) to simultaneously disrupt both DGAT enzymes. The DGAT2-/- MEFs exhibited a low amount of LDs under basal conditions, which increased dramatically after a 6-h treatment with 200 µM oleate (Figure 5, B and C), indicating that DGAT2-/- MEFs are still able to generate LDs in response to an oleate challenge, due to the presence of DGAT1. Treatment with either triacsin C or DGAT1i reduced the amount of LDs in non–oleate-treated cells and completely blocked the increase in LD biogenesis in response to oleate (Figure 5, B and C). The levels of the LD protein perilipin-2 (PLIN2) are known to correlate with LD abundance, and, in the absence of LDs, PLIN2 is degraded by the ubiquitin-proteasome system (Xu *et al.*, 2005; Masuda *et al.*, 2006; Takahashi *et al.*, 2016). Analysis of PLIN2 levels and cellular distribution indicate that triacsin C and DGAT1i treatments block oleate-induced increases in PLIN2 levels and PLIN2-immunoreactive LDs (Supplemental Figure S4). Together these data demonstrate that the DGAT2-/- MEFs provide a facile means to acutely manipulate LD biogenesis at an upstream step (i.e., with triacsin C) or a downstream step (i.e., with DGAT1 inhibitor).

As observed in HEK293 cells, CD147(CG) was degraded in DGAT2-/- MEFs during an emetine translation shutoff experiment and was stabilized by a triacsin C pretreatment (Figure 5, D and E). The rate of CD147(CG) degradation was greater in the DGAT2-/- MEFs than in the HEK293 cells (half-life ~25 min vs. ~2 h). DGAT1i pretreatment, despite inhibiting LD biogenesis (Figure 5, B and C), had no effect on the kinetics of CD147 degradation (Figure 5, D and E). These results argue against a requirement for LDs in CD147 degradation and suggest that triacsin C affects ERAD through a mechanism independent of LDs.

Metabolomic profiling reveals global alterations in the cellular lipid landscape of triacsin C–treated cells

To understand the effects of triacsin C on cellular lipid homeostasis, we performed targeted single reaction monitoring (SRM)–based liquid chromatography–tandem mass spectrometry (LC-MS/MS) steady-state lipidomic profiling of >100 lipid metabolites, encompassing a wide array of lipid classes, including neutral lipids, fatty acids, acyl carnitines (ACs), N-acyl ethanolamines, sterols, phospholipids, sphingolipids, lysophospholipids, and ether lipids (Figure 6 and Supplemental Table S3). Among the 118 lipids, 71 exhibited significant changes ($p < 0.05$) after a 16-h triacsin C treatment (Figure 6, A–K). As expected, we observed a prominent decrease in the levels of many neutral lipids—monoacylglycerols (MAGs), diacylglycerols (DAGs), and TAGs (Figure 6, B and C). Not all species of TAG were reduced (e.g., C16:0/C20:4/C16:0 TAG

and C18:0/C18:0/C18:0 TAG; Figure 6, B and C), suggesting that there may be protected pools of TAGs or that some ACSLs that are incompletely inhibited mediate the formation of these specific TAGs (Igal *et al.*, 1997). We also observed an anticipated decrease in AC levels, particularly in C16:0 AC (Figure 6, B and E). Although free fatty acids might be expected to accumulate due to the inhibition of ACSLs and consequent lack of conversion into the CoA intermediate for cellular use, no changes in fatty acid levels were detected (Figure 6B). This may be due to a compensatory efflux of free fatty acids (Igal *et al.*, 1997), which could result in an underestimate of total free fatty acid levels, or increased flux through ACSL enzymes that are not inhibited.

Broad changes in additional cellular lipids were also observed, including decreases in many phospholipids, phospholipid ethers, neutral ether lipids, and lysophospholipid ethers (Figure 6, B–K). The decreases in lipid levels presumably resulted from impairments in synthesis caused by the inability of ACSLs to activate fatty acids, a requirement for conjugation. Particularly striking was the general decrease in nearly all phosphatidylinositol and phosphatidylinositol ether lipids (Figure 6, B, F, and J). This is interesting, given the recent finding that phosphatidylinositol maintains ER homeostasis in yeast by sequestering fatty acids when LD biogenesis is inhibited (Velázquez *et al.*, 2016). Our results suggest that phosphatidylinositol may represent an especially dynamic phospholipid pool that reflects the levels of fatty acid flux.

Several lipid species displayed significant increases, including many lysophospholipids (Figure 6, B, D, and H), which can act as signaling molecules, and several phospholipids (Figure 6, B–K). The increase in some lipids is consistent with the possible increased flux of fatty acids through ACSL enzymes that are not inhibited or are incompletely inhibited by triacsin C. The ratio of phosphatidylcholine (PC) to phosphatidylethanolamine (PE) has been implicated in ER homeostasis (Li *et al.*, 2006; Fu *et al.*, 2011; Thibault *et al.*, 2012), and although we observed alterations in PC and PE levels (Figure 6, B and F), the ratio between the two lipid species was relatively unchanged. An increase in ceramides (C16:0 ceramide and C18:0 ceramide) was detected (Figure 6, B and G), which is notable, given their role in cellular stress responses and UPR activation (Volmer and Ron, 2015). Together our results indicate that triacsin C treatment not only affects the levels of neutral lipids sequestered in LDs, but it also causes widespread alterations in the cellular lipid landscape (Figure 6). The levels of several of the altered lipids have been suggested to affect ER homeostasis (e.g., phosphosphatidylinositol and ceramides).

Triacsin C activation of the PERK and IRE1 arms of the UPR has opposing effects on cell viability

Disruptions in ERAD and in lipid homeostasis can activate the UPR (Jonikas *et al.*, 2009; Volmer and Ron, 2015). Inositol-requiring enzyme-1 (IRE1), an ER transmembrane serine/threonine kinase and endonuclease, is a primary mediator of the UPR that splices XBP1 mRNA to enable the translation of the XBP1 transcription factor (Walter and Ron, 2011). Analysis using reverse transcription PCR revealed that incubation with triacsin C induced XBP1 splicing (Figure 7A). The spliced form of XBP1 was detectable at low levels as early as 8 h, and it became much more prominent at 16 and 24 h (Figure 7A). A second arm of the UPR is controlled by the ER-resident kinase PKR-like ER kinase (PERK), which phosphorylates the α subunit of eukaryotic translation-initiation factor 2 (eIF2α). Phosphorylation of eIF2α represses global translation while simultaneously promoting the translation of the ATF4 transcription factor to up-regulate stress-responsive genes such as the proapoptotic transcription factor C/EBP homologous protein (CHOP; Hiramatsu *et al.*, 2015). To examine the potential effect of triacsin C on PERK induction of stress-responsive genes, we exploited a clonal HEK293 reporter cell line expressing an 8.5-kb CHOP gene fragment fused to GFP (CHOP::GFP; Wang *et al.*, 1998; Novoa *et al.*, 2001). Treatment with tunicamycin, an inhibitor of N-linked glycosylation that induces the UPR, resulted in a robust and rapid accumulation in GFP fluorescence (Figure 7C and Supplemental Figure S5). Treatment with triacsin C also caused an increase in GFP fluorescence but with different temporal dynamics. During the first 8 h, no increase in GFP fluorescence was observed (Figure 7C). This lag period was followed by an increase in GFP fluorescence levels at 16 and 24 h (Figure 7C).

The IRE1 and PERK arms of the UPR play well-characterized protective roles through the induction of genes involved in protein folding and membrane expansion and through the repression of translation (Walter and Ron, 2011). Of note, UPR up-regulation protected yeast from ER trafficking and ERAD defects induced by lipid disequilibrium (Thibault *et al.*, 2012). However, persistent activation of IRE1 or PERK can lead to cell death (Lin *et al.*, 2007; Han *et al.*, 2009). To determine the role of the IRE1 and PERK pathways in the cellular response to triacsin C treatment, we analyzed the effects of the IRE1 inhibitor 4μ8c (IRE1i) and PERK inhibitor GSK2606414 (PERKi). IRE1i completely blocked triacsin C–induced XBP1 cleavage (Figure 7, A and B), and PERKi significantly attenuated the induction of the CHOP::GFP reporter (Figure 7D). Inhibition of PERK increased the amounts of cell death induced by triacsin C at 8, 16, and 24 h (Figure 7E), indicating that PERK plays a predominantly protective role under these conditions. In contrast, inhibition of IRE1 had little effect during triacsin C treatment and increased the amount of cell death at 24 h (Figure 7E). These findings indicate that both the IRE1 and PERK arms of the UPR are induced by triacsin C, but that the outputs of these two signaling pathways have opposing effects on cell viability.

DISCUSSION

Although there are several intriguing connections between LDs and ERAD, whether LDs are directly involved in the ERAD mechanism has remained an outstanding question. Our data argue that LD biogenesis is not a fundamental requirement for ERAD. Instead, our results support a model (Figure 7F) in which triacsin C inhibition of ACSLs causes widespread changes in the cellular lipid composition that impair specific steps in ERAD, resulting in disruptions in ER proteostasis, activation of the UPR, and eventual cell death. Thus, dysregulated fatty acid metabolism negatively affects ER homeostasis and protein quality control independently of LDs.

To inhibit LD biogenesis but avoid the broad effects that ACSL inhibition has on lipid homeostasis, we pursued an approach that would disrupt a downstream step in TAG synthesis. To this end, we characterized a combined chemical (DGAT1 inhibition) and genetic (DGAT2-/-) approach to inhibit both of the DGAT enzymes, which are required for the conversion of DAG to TAG and the generation of LDs (Yen *et al.*, 2008; Harris *et al.*, 2011). This strategy enabled acute disruption of LD biogenesis, reducing LD abundance under basal and oleate-stimulated conditions as effectively as triacsin C does. In contrast to triacsin C, disruption of LD biogenesis by inhibiting the DGATs had no effect on the kinetics of CD147 ERAD. These results are consistent with previous analyses of ERAD in yeast models of LD disruption (Olzmann and Kopito, 2011; Nakatsukasa and Kamura, 2016), which together demonstrate that LD biogenesis is not integral to the ERAD mechanism in yeast or mammalian cells. The possibility that LDs may function in the degradation of specific substrates or in ERAD under specific conditions is still worth consideration. For

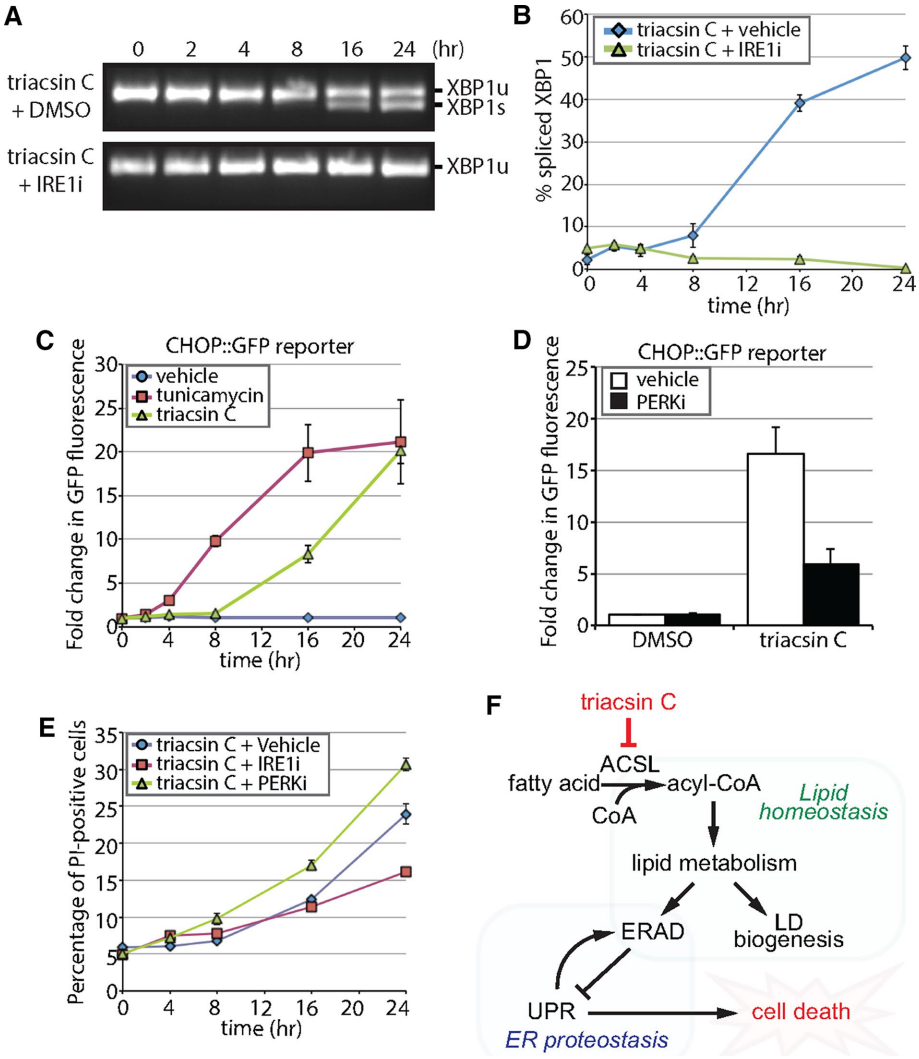

FIGURE 7: Triacsin C activates opposing arms of the UPR. (A) Reverse transcription PCR assay of XBP1 mRNA from HEK293 cells treated with 1 μg/ml triacsin C for the indicated times in the presence and absence of 100 μM IRE1 inhibitor 4μ8c (IRE1i). XBP1 amplicons were separated on an agarose gel and imaged. XBP1u, unspliced XBP1; XBP1s, spliced XBP1. (B) Quantification of the percentage of spliced XBP1 in A ($n = 3$). (C) HEK293 cells stably expressing a CHOP::GFP construct were treated with vehicle, 1 μg/ml triacsin C, or 5 μg/ml tunicamycin as indicated and GFP levels measured using flow cytometry. The fold change in GFP fluorescence relative to time 0 h is shown ($n = 3$). (D) HEK293 cells stably expressing a CHOP::GFP construct were treated with vehicle or 1 μg/ml triacsin C for 0 and 16 h in the presence and absence of 1 μM PERK inhibitor GSK2606414 (PERKi). GFP levels were measured using flow cytometry. The fold change in GFP fluorescence relative to time 0 h is shown ($n = 3$). (E) HEK293 cells were treated with 1 μg/ml triacsin C and vehicle, 100 μM IRE1i, or 1 μM PERKi for the indicated times and stained with propidium iodide to identify apoptotic cells. The percentage of apoptotic cells relative to time 0 h is shown ($n = 3$). (F) A model depicting the relationship between fatty acid metabolism and ER proteostasis. Disruptions in fatty acid metabolism result in lipid disequilibrium, causing impairments in ER quality control by inhibiting specific steps in ERAD (independent of LDs). The disruption in ER homeostasis activates the UPR, which protects cells via the PERK pathway and eventually kills cells via the IRE1 pathway. Error bars indicate SEM.

example, for ApoB100, an extremely large, hydrophobic protein, the association with LDs might provide a specialized ERAD mechanism to reduce aggregation (Ohsaki *et al.*, 2006; Suzuki *et al.*, 2012). LDs may also contribute to ERAD only under particular conditions, such as periods of disrupted proteostasis. Under conditions in which proteasomal capacity is limiting, the LD surface could act as a transient site for the sequestration of ERAD and other UPS substrates (Ohsaki *et al.*, 2006; Vevea *et al.*, 2015).

Our findings are in agreement with previous reports that triacsin C impairs ERAD (Hartman *et al.*, 2010; Klemm *et al.*, 2011; Jo *et al.*, 2013). Indeed, we found that triacsin C inhibited the degradation of two glycosylated Hrd1 substrates—the luminal substrate NHK and the endogenous integral membrane substrate CD147. The highest amount of substrate stabilization required a 16-h pretreatment with triacsin C, suggesting that ACSL activity is not required acutely during ERAD but instead that ACSL activity is required to establish a particular cellular environment conducive for ERAD. To define more precisely the step in ERAD that is affected by triacsin C, we tested individual steps of ERAD in the context of triacsin C treatment. Our results indicate that the triacsin C–induced defect in protein degradation is upstream of the proteasome and is confined to a subset of ERAD pathways. This conclusion is supported by several findings: 1) ubiquitinated proteins did not accumulate in response to triacsin C, 2) triacsin C did not stabilize a cytosolic UPS substrate, 3) triacsin C affected a subset of ERAD substrates—CD147 and NHK—but not CFTRΔF508, and 4) triacsin C impaired the dislocation of a luminal glycosylated substrate. Moreover, analyses of the glycosylation state of CD147 during degradation indicate that triacsin C treatment impaired CD147 glycan trimming and delivery to the Hrd1 complex, suggesting that the primary impairment in ERAD is due to the failure to expose the trimmed glycan structure necessary for degradation commitment. Our proteomics data indicate that the composition of the Hrd1 complex is largely unaltered in triacsin C–treated cells; however, it is possible that alterations in the ER lipid composition could modulate the structure and/or function of the complex. The enzymes involved in the trimming of CD147's glycans are unknown, but this step is most likely catalyzed by ER-resident mannosidases ERManI and/or EDEM1-3. Disruptions in lipid composition could influence substrate localization to ERManI-containing ER subdomains (Benyair *et al.*, 2015) or could affect EDEM membrane association, which is known to affect EDEM glycan trimming activity toward certain substrates (Tamura *et al.*, 2011). It is also possible that the inhibition of ACSLs could influence protein acylation, and both calnexin (Lakkaraju *et al.*, 2012; Lynes *et al.*, 2012, 2013) and the ERAD E3 ligase gp78 (Fairbank *et al.*, 2012) have been reported to be palmitoylated. Whether other ERAD factors are regulated by lipid modifications is unknown.

Activation of the UPR initiates signaling pathways with opposing outputs, a protective response that seeks to reestablish ER homeostasis and an apoptotic response that promotes cell death in the face of persistent ER stress (Lin *et al.*, 2007, 2009; Hetz, 2012;

Lu *et al.*, 2014). Consistent with disruptions in ER homeostasis, treatment with triacsin C induced XBP1 splicing (IRE1 arm) and CHOP::GFP expression (PERK arm) and eventually caused cell death. Treatment of cells with the UPR inducer tunicamycin causes a rapid and transient up-regulation of IRE1 signaling that is paralleled by a slower increase in apoptotic PERK signaling at later times (Lin *et al.*, 2007). Of interest, in response to triacsin C, we see very different temporal dynamics and effects of UPR induction. Both the PERK and IRE1 arms exhibited similar activation kinetics and, after an initial lag period, steadily increased until the end of our experiments. Despite increasing CHOP reporter expression, PERK actions were overall protective in response to triacsin C. This finding indicates that CHOP expression alone is not conclusive evidence of a proapoptotic signaling output, consistent with the observation that forced CHOP expression was insufficient to induce cell death (Han *et al.*, 2013). In contrast to PERK, IRE1 signaling appeared to promote cell death, and the inhibition of IRE1 attenuated triacsin C–induced apoptosis, possibly by inhibiting excessive regulated Ire1-dependent decay (RIDD) of important secretory transcripts (Han *et al.*, 2009) or activation of a JNK apoptotic signaling pathway (Urano *et al.*, 2000). These results highlight the complex relationship between the UPR and cell death and reveal that the mode of UPR activation (e.g., tunicamycin vs. triacsin C) has a profound effect on the ultimate effects of each UPR branch. Alterations in phospholipids can directly induce UPR signaling (Volmer *et al.*, 2013; Volmer and Ron, 2015), and whether the changes in the lipid environment, the defects in ER protein quality control, or both are responsible for triacsin C activation of the UPR is unclear. In addition, how the UPR is customized to fit a particular ER stressor is not evident. It is possible that the temporal coordination of individual UPR branches influences the end output (i.e., protection vs. cell death) or that different ER stressors provide a unique "second hit" (e.g., disruptions in lipid homeostasis or depletion in ER calcium pools) that sensitizes cells to IRE1- or PERK-dependent cell death pathways.

Our study reveals an intimate relationship between cellular lipid homeostasis and ER protein quality control. Our findings raise the possibility that certain lipid environments and/or modifications may affect ER proteostasis by regulating specific steps of the ERAD process. It is worth noting that a multitude of diseases, ranging from obesity to neurodegenerative diseases, are associated with altered lipid homeostasis and upregulated UPR (Hetz *et al.*, 2013). In addition, targeting lipid metabolic enzymes to decrease fatty acid availability (e.g., inhibition of FASN) is being actively pursued as a therapeutic strategy for the treatment of cancer (Menendez and Lupu, 2007; Currie *et al.*, 2013; Benjamin *et al.*, 2015). Therefore, elucidating the connections between ER lipid and protein homeostasis could have significant ramifications for our understanding of the pathogenic mechanisms underlying a wide number of diseases.

MATERIALS AND METHODS

Plasmids, antibodies, and reagents

The pcDNA3.1(-) plasmids for expression of TTR-HA, the null Hong Kong mutant of α-1 antitrypsin (NHK-HA and NHK-GFP), and S-tagged Hrd1 (Hrd1-S) were previously described (Christianson *et al.*, 2008, 2012). The CFTRΔF508 plasmid was kindly provided by Doug Cyr (University of North Carolina at Chapel Hill, Chapel Hill, NC).

Antibodies employed in this study include anti-CD147 (A-12, G-19, 8D6; Santa Cruz Biotechnology), anti-Hrd1 (A302-946A; Bethyl), anti-HA (HA7; Sigma-Aldrich), anti–S-peptide (EMD Millipore), anti-tubulin (Abcam), anti–glyceraldehyde-3-phosphate dehydrogenase (EMD Millipore), anti-GFP (Roche), anti-CFTR (University of North Carolina at Chapel Hill, CFTR Antibodies Distribution Program), anti–ubiquitin conjugates (FK2; EMD Millipore), anti-AUP1 (Proteintech), anti-SEL1L (T-17; Santa Cruz Biotechnology) and anti-KDEL (Enzo). Anti–derlin-1 and anti–derlin-2 antibodies were kind gifts from Yihong Ye (National Institutes of Health, Bethesda, MD). Rabbit polyclonal anti-UBXD8 antibodies were generated against a histidine-tagged fragment of UBXD8 (amino acids 97–445) by Proteintech Group. All IRDye680- and IRDye800-conjugated secondary antibodies for Western blotting were obtained from LI-COR. Alexa Fluor–conjugated secondary antibodies for immunofluorescence microscopy were obtained from Thermo Fisher Scientific.

Reagents employed in this study include triacsin C (Enzo Life Sciences), emetine dihydrochloride hydrate (Sigma-Aldrich), CB-5083 (Anderson *et al.*, 2015; Cleave Biosciences), oleate (Sigma-Aldrich), kifunensine (Cayman Chemical), deoxynojirimycin (Sigma-Aldrich), MG-132 (Selleck Chemicals), T863 (Sigma-Aldrich), 4μ8C (EMD Millipore), GSK2606414 (EMD Millipore), tunicamycin (Cayman Chemical), and PNGase F (New England Biolabs).

Cell culture and transfections

HEK293, HEK293T, MEF, HeLa, and U2OS cells were cultured in DMEM containing 4.5 g/l glucose and L-glutamine (Corning) supplemented with 10% fetal bovine serum (FBS) (Thermo Fisher Scientific and Gemini Bio Products) at 37°C and 5% CO_2. 293T.FluERAD cells stably expressing a split-Venus system for the analysis of the dislocation step of ERAD (Grotzke *et al.*, 2013) were kindly provided by Peter Cresswell (Yale University, New Haven, CT). U2OS cells stably expressing Venus-DD (Bersuker *et al.*, 2016) and HEK293 cells stably expressing the CHOP::GFP reporter were kindly provided by Ron Kopito (Stanford University, Stanford, CA). DGAT2-/- MEF cells were kindly provided by Robert Farese, Jr. (Harvard University, Cambridge, MA). All plasmid transfections were performed using X-tremeGENE HP (Roche) transfection reagent according to the manufacturer's instructions.

Immunoblotting analysis

Cells were washed extensively in phosphate-buffered saline (PBS) and lysed in 1% SDS. Protein amounts were normalized using a bicinchoninic acid (BCA) protein assay (Thermo Fisher Scientific). Proteins were separated on 4–20% polyacrylamide gradient gels (Bio-Rad) and transferred onto low-fluorescence polyvinylidene fluoride or nitrocellulose membranes (Bio-Rad). Large-format gel electrophoresis was performed using 10% acrylamide gels made with acrylamide/bis 19:1. Membranes were incubated in 5% nonfat milk in PBS plus 0.1% Tween-20 (PBST) for 30 min to reduce nonspecific antibody binding. Membranes were then incubated for at least 2 h in PBST containing 5% milk or 1% bovine serum albumin (BSA; Sigma-Aldrich) and primary antibodies, followed by incubation for at least 1 h in PBST containing 1% BSA and fluorescence-conjugated secondary antibodies. Immunoblots were visualized on a LI-COR imager (LI-COR Biosciences), and ImageJ (Schneider *et al.*, 2012) was used for quantification.

Immunofluorescence microscopy

HeLa and MEF cells were plated on poly-L-lysine–coated coverslips. Cells were treated the next day, washed with PBS, and fixed at room temperature with 4% paraformaldehyde in PBS for 10 min. Cells were washed three times with PBS and permeabilized with 0.1% Triton X-100 plus 1% BSA in PBS at room temperature for 30 min. Cells were washed three times with 1% BSA in PBS and incubated for 2 h in primary antibodies, washed three times, and incubated for 1 h with Alexa Fluor–conjugated secondary antibodies, BODIPY493/503 (LD staining; Thermo Fisher Scientific),

and 4′,6-diamidino-2-phenylindole (DAPI; nuclei staining; Thermo Fisher Scientific). Cells were washed three times and mounted using Fluoromount-G (SouthernBiotech). Cells were visualized using a DeltaVision Elite microscope and acquired images deconvolved and analyzed using SoftWoRx. The abundance of LDs per cell was determined by measuring the area of BODIPY493/503–stained LDs per cell using ImageJ (Schneider *et al.*, 2012).

Affinity purifications

HEK293 cells were harvested, washed with PBS, and lysed in immunoprecipitation (IP) buffer (50 mM Tris-HCl, pH 7.5, 150 mM NaCl, 1% digitonin, and protease inhibitor tablets [Thermo Fisher Scientific]) at 4°C for 30 min. Lysates were clarified by centrifugation at 20,000 × *g* for 10 min. Protein concentrations were measured using the BCA assay. For the affinity purification of S-tagged protein complexes, lysates were loaded onto S-protein agarose beads (EMD Millipore) at a concentration of 25 µl beads per 1 mg of lysate. For endogenous Hrd1 IPs, 2 mg of lysate was incubated with anti-Hrd1 antibodies for 1 h and then loaded onto 25 µl of protein G agarose beads (EMD Millipore). Lysates were incubated with the beads rotating at 4°C for 2 h, washed three times with lysis buffer containing 0.1% digitonin, and eluted in loading buffer.

Radiolabeling and pulse-chase analysis

HEK293 cells plated on poly-L-lysine–coated plates were washed twice with "cold" medium, which lacked L-methionine and L-cysteine and contained 10% dialyzed FBS, and then starved in this medium for 30 min. Cells were radiolabeled in medium containing 125 µCi/ml ^{35}S-labeled cysteine/methionine (Easytag Express Protein Labeling Mix 35S; PerkinElmer) for 30 min, washed twice with Hanks' buffered saline solution, and then chased in complete medium containing 75 µM emetine for the indicated times. Cells were harvested, collected by centrifugation, washed in PBS, and lysed in pulse-chase IP buffer (25 mmol/l 4-(2-hydroxyethyl)-1-piperazineethanesulfonic acid buffer, pH 7.4, 150 mmol/l NaCl, 5 mmol/l $MgCl_2$, 1% 3-[(3-cholamidopropyl)dimethylammonio]-1-propanesulfonate detergent, and protease inhibitors). Lysates were cleared by centrifugation at 20,000 × *g* for 15 min at 4°C and protein concentrations determined using the BCA assay. Lysates were precleared with protein G beads (EMD Millipore). CD147 was immunoprecipitated from lysates by incubation with anti-CD147 antibody (8D6; Santa Cruz biotechnology) for 4 h at 4°C with mixing, followed by incubation with protein G beads (EMD Millipore) for an additional 2 h at 4°C with mixing. Immunoprecipitated proteins were washed thrice with the pulse-chase IP buffer and then separated by SDS–PAGE. Gels were dried and exposed to a Storage Phosphor Screen (GE Healthcare Life Sciences) for 16 h at room temperature. Radioactive signals corresponding to CD147(Mat.) and CD147(CG) were detected using a Typhoon 9400 Molecular Imager (GE Healthcare Life Sciences).

SILAC mass spectrometry

Parental HEK293 cells or HEK293 cells expressing S-tagged Hrd1 were grown in DMEM lacking L-arginine and L-lysine supplemented with 10% dialyzed FBS (Life Technologies) and the appropriate SILAC amino acids: *light*, L-arginine (Arg0) and L-lysine (Lys0); *medium*, $^{13}C_6$-L-arginine (Arg6) and 4,4,5,5-D_4-L-lysine (Lys4); and *heavy,* $^{13}C_6{}^{15}N_4$-L-arginine (Arg10) and $^{13}C_6{}^{15}N_2$-L-lysine (Lys8). Cells were cultured for at least seven cell doublings to allow for complete incorporation of the stable isotope-labeled amino acids (Cambridge Isotope Laboratories). Parental HEK293 control cells were *light* SILAC labeled, and S-tagged Hrd1 cells were either *medium* or *heavy* labeled. At 16 h before harvest, the S-tagged Hrd1 cells were incubated with either vehicle (*medium* SILAC labeled) or 1 µg/ml triacsin C (*heavy* SILAC labeled). After several washes in PBS, cells were lysed in IP buffer, and 3 mg of protein lysate was loaded onto 75 µl of S-protein agarose beads (EMD Millipore). Lysates were rotated at 4°C for 2 h and washed three times with IP buffer containing 0.1% digitonin and twice with 50 mM ammonium bicarbonate. Beads were resuspended in 75 µl of 0.2% RapiGest SF (Waters) in 50 mM ammonium bicarbonate for 15 min at 65°C, followed by incubation with 2.5 µg of trypsin (Thermo Fisher Scientific) overnight at 37°C. The affinity purification for each condition was performed separately to prevent exchange of interaction partners during the incubations. After the proteolysis step, equal volumes of digested peptides were combined and acidified with HCl to pH 2.0. Rapigest SF precipitate was removed by centrifugation at 20,000 × *g* for 30 min and the peptide solution concentrated to 40 µl using a SpeedVac. Digested peptides were analyzed by LC-MS/MS on a Thermo Scientific Q Exactive Orbitrap Mass spectrometer in conjunction with a Proxeon Easy-nLC II HPLC (Thermo Fisher Scientific) and Proxeon nanospray source at the University of California, Davis, Proteomics Core Facility. The digested peptides were loaded onto a 100 µm × 25 mm Magic C18 100-Å 5U reverse-phase trap, where they were desalted online before being separated using a 75 µm × 150 mm Magic C18 200-Å 3U reverse-phase column. Peptides were eluted using a 180-min gradient with a flow rate of 300 nl/min. An MS survey scan was obtained for the *m/z* range 300–1600, and MS/MS spectra were acquired using a top 15 method, in which the top 15 ions in the MS spectra were subjected to high-energy collisional dissociation. An isolation mass window of 1.6 *m/z* was used for the precursor ion selection, and a normalized collision energy of 27% was used for fragmentation. A 5-s duration was used for the dynamic exclusion. The acquired MS/MS spectra were searched against a full UniProt database of human protein sequences, and SILAC ratios were determined using MaxQuant. The mass spectrometry proteomics data have been deposited to the ProteomeXchange Consortium via the PRIDE partner repository with the data set identifier PXD005633.

Lipidomic profiling

HEK293 cells were grown to 70% confluence in a 10-cm dish and treated for 16 h with vehicle or 1 µg/ml triacsin C. Cells were washed twice with PBS and harvested, and cell pellets were stored at –80°C. Lipid metabolite extraction and analysis by SRM-based LC-MS/MS was performed as previously described (Benjamin *et al.*, 2013, 2015; Mulvihill *et al.*, 2014). Briefly, nonpolar lipid metabolites were extracted in 2:1:1 chloroform/methanol/PBS supplemented with internal standards C12:0 dodecylglycerol (10 nmol) and pentadecanoic acid (10 nmol). The organic and aqueous layers were collected after separation by centrifugation at 1000 × *g* for 5 min. The aqueous layer was acidified by addition of 0.1% formic acid and subjected to a second chloroform extraction. The resulting organic layers were combined and mixed, dried down under N_2, and dissolved in 120 µl of chloroform. A 10-µl aliquot was analyzed by SRM LC-MS/MS. Metabolites were separated using a Luna reverse-phase C5 column (Phenomenex), and MS analysis was performed on an Agilent 6430 QQQ LC-MS/MS. Quantification of metabolites was performed by integrating the area under the peak, normalized to internal standard values, adjusted based on external standard curves, and expressed as relative levels compared with the control sample.

XBP1 splicing assay

RNA was isolated using TRIzol Reagent (Life Technologies) and cDNA generated using the High-Capacity cDNA Reverse Transcription Kit

(Applied Biosystems) according to the manufacturer's directions. XBP1 was amplified using the primers 5′-AAACAGAGTAGCAGC-TCAGACTGC-3′ and 5′-TCCTTCTGGGTAGACCTCTGGGAG-3′. Amplified products were separated on a 2.5% agarose gel at 80 V for 2 h and visualized using a Gel Doc imaging system (Bio-Rad).

Cell viability

Cells were trypsinized, pelleted by centrifugation at 500 × *g* for 5 min, washed in PBS, and resuspended in 100 µl of PBS containing 2.5 µg/ml propidium iodide (BD Biosciences). After a 5-min incubation, cells were diluted with PBS to a final volume of 1 ml and analyzed using a BD Biosciences LSRFortessa. Cell suspensions were stored on ice throughout the procedure. Subsequent data analysis was performed using FlowJo software.

ACKNOWLEDGMENTS

We thank John Christianson, Ethan Greenblatt, Ron Kopito, and Christopher Walczak for critical reading of the manuscript and the members of the Olzmann lab for helpful discussions. This research was supported by grants from the National Institutes of Health (R00DK095921 and R01GM112948 to J.A.O.).

REFERENCES

Adeyo O, Horn PJ, Lee S, Binns DD, Chandrahas A, Chapman KD, Goodman JM (2011). The yeast lipin orthologue Pah1p is important for biogenesis of lipid droplets. J Cell Biol 192, 1043–1055.

Anand P, Cermelli S, Li Z, Kassan A, Bosch M, Sigua R, Huang L, Ouellette AJ, Pol A, Welte MA, *et al.* (2012). A novel role for lipid droplets in the organismal antibacterial response. Elife 1, e00003.

Anderson DJ, Le Moigne R, Djakovic S, Kumar B, Rice J, Wong S, Wang J, Yao B, Valle E, Kiss von Soly S, *et al.* (2015). Targeting the AAA ATPase p97 as an approach to treat cancer through disruption of protein homeostasis. Cancer Cell 28, 653–665.

Baldridge RD, Rapoport TA (2016). Autoubiquitination of the Hrd1 ligase triggers protein retrotranslocation in ERAD. Cell 166, 394–407.

Banaszynski LA, Chen LC, Maynard-Smith LA, Ooi AG, Wandless TJ (2006). A rapid, reversible, and tunable method to regulate protein function in living cells using synthetic small molecules. Cell 126, 995–1004.

Benjamin DI, Cozzo A, Ji X, Roberts LS, Louie SM, Mulvihill MM, Luo K, Nomura DK (2013). Ether lipid generating enzyme AGPS alters the balance of structural and signaling lipids to fuel cancer pathogenicity. Proc Natl Acad Sci USA 110, 14912–14917.

Benjamin DI, Li DS, Lowe W, Heuer T, Kemble G, Nomura DK (2015). Diacylglycerol metabolism and signaling is a driving force underlying FASN inhibitor sensitivity in cancer cells. ACS Chem Biol 10, 1616–1623.

Benyair R, Ogen-Shtern N, Lederkremer GZ (2015). Glycan regulation of ER-associated degradation through compartmentalization. Semin Cell Dev Biol 41, 99–109.

Bersuker K, Brandeis M, Kopito RR (2016). Protein misfolding specifies recruitment to cytoplasmic inclusion bodies. J Cell Biol 213, 229–241.

Bogdanov M, Mileykovskaya E, Dowhan W (2008). Lipids in the assembly of membrane proteins and organization of protein supercomplexes: implications for lipid-linked disorders. Subcell Biochem 49, 197–239.

Brasaemle DL, Dolios G, Shapiro L, Wang R (2004). Proteomic analysis of proteins associated with lipid droplets of basal and lipolytically stimulated 3T3-L1 adipocytes. J Biol Chem 279, 46835–46842.

Caldwell SR, Hill KJ, Cooper AA (2001). Degradation of endoplasmic reticulum (ER) quality control substrates requires transport between the ER and Golgi. J Biol Chem 276, 23296–23303.

Cao J, Zhou Y, Peng H, Huang X, Stahler S, Suri V, Qadri A, Gareski T, Jones J, Hahm S, *et al.* (2011). Targeting Acyl-CoA:diacylglycerol acyltransferase 1 (DGAT1) with small molecule inhibitors for the treatment of metabolic diseases. J Biol Chem 286, 41838–41851.

Carvalho P, Stanley AM, Rapoport TA (2010). Retrotranslocation of a misfolded luminal ER protein by the ubiquitin-ligase Hrd1p. Cell 143, 579–591.

Cermelli S, Guo Y, Gross SP, Welte MA (2006). The lipid-droplet proteome reveals that droplets are a protein-storage depot. Curr Biol 16, 1783–1795.

Cherepanova N, Shrimal S, Gilmore R (2016). N-linked glycosylation and homeostasis of the endoplasmic reticulum. Curr Opin Cell Biol 41, 57–65.

Christianson JC, Olzmann JA, Shaler TA, Sowa ME, Bennett EJ, Richter CM, Tyler RE, Greenblatt EJ, Harper JW, Kopito RR (2012). Defining human ERAD networks through an integrative mapping strategy. Nat Cell Biol 14, 93–105.

Christianson JC, Shaler TA, Tyler RE, Kopito RR (2008). OS-9 and GRP94 deliver mutant alpha1-antitrypsin to the Hrd1-SEL1L ubiquitin ligase complex for ERAD. Nat Cell Biol 10, 272–282.

Christianson JC, Ye Y (2014). Cleaning up in the endoplasmic reticulum: ubiquitin in charge. Nat Struct Mol Biol 21, 325–335.

Contreras FX, Ernst AM, Wieland F, Brügger B (2011). Specificity of intramembrane protein-lipid interactions. Cold Spring Harb Perspect Biol 3, a004705.

Currie E, Schulze A, Zechner R, Walther TC, Farese RV (2013). Cellular fatty acid metabolism and cancer. Cell Metab 18, 153–161.

Egeler EL, Urner LM, Rakhit R, Liu CW, Wandless TJ (2011). Ligand-switchable substrates for a ubiquitin-proteasome system. J Biol Chem 286, 31328–31336.

Fairbank M, Huang K, El-Husseini A, Nabi IR (2012). RING finger palmitoylation of the endoplasmic reticulum Gp78 E3 ubiquitin ligase. FEBS Lett 586, 2488–2493.

Fei W, Wang H, Fu X, Bielby C, Yang H (2009). Conditions of endoplasmic reticulum stress stimulate lipid droplet formation in Saccharomyces cerevisiae. Biochem J 424, 61–67.

Fu S, Yang L, Li P, Hofmann O, Dicker L, Hide W, Lin X, Watkins SM, Ivanov AR, Hotamisligil GS (2011). Aberrant lipid metabolism disrupts calcium homeostasis causing liver endoplasmic reticulum stress in obesity. Nature 473, 528–531.

Fujimoto Y, Itabe H, Kinoshita T, Homma KJ, Onoduka J, Mori M, Yamaguchi S, Makita M, Higashi Y, Yamashita A, *et al.* (2007). Involvement of ACSL in local synthesis of neutral lipids in cytoplasmic lipid droplets in human hepatocyte HuH7. J Lipid Res 48, 1280–1292.

Garbarino J, Padamsee M, Wilcox L, Oelkers PM, D'Ambrosio D, Ruggles KV, Ramsey N, Jabado O, Turkish A, Sturley SL (2009). Sterol and diacylglycerol acyltransferase deficiency triggers fatty acid-mediated cell death. J Biol Chem 284, 30994–31005.

Greenblatt EJ, Olzmann JA, Kopito RR (2011). Derlin-1 is a rhomboid pseudoprotease required for the dislocation of mutant α-1 antitrypsin from the endoplasmic reticulum. Nat Struct Mol Biol 18, 1147–1152.

Grotzke JE, Lu Q, Cresswell P (2013). Deglycosylation-dependent fluorescent proteins provide unique tools for the study of ER-associated degradation. Proc Natl Acad Sci USA 110, 3393–3398.

Guerriero CJ, Brodsky JL (2012). The delicate balance between secreted protein folding and endoplasmic reticulum-associated degradation in human physiology. Physiol Rev 92, 537–576.

Haemmerle G, Moustafa T, Woelkart G, Büttner S, Schmidt A, van de Weijer T, Hesselink M, Jaeger D, Kienesberger PC, Zierler K, *et al.* (2011). ATGL-mediated fat catabolism regulates cardiac mitochondrial function via PPAR-α and PGC-1. Nat Med 17, 1076–1085.

Han D, Lerner AG, Vande Walle L, Upton JP, Xu W, Hagen A, Backes BJ, Oakes SA, Papa FR (2009). IRE1alpha kinase activation modes control alternate endoribonuclease outputs to determine divergent cell fates. Cell 138, 562–575.

Han GS, O'Hara L, Carman GM, Siniossoglou S (2008). An unconventional diacylglycerol kinase that regulates phospholipid synthesis and nuclear membrane growth. J Biol Chem 283, 20433–20442.

Han J, Back SH, Hur J, Lin YH, Gildersleeve R, Shan J, Yuan CL, Krokowski D, Wang S, Hatzoglou M, *et al.* (2013). ER-stress-induced transcriptional regulation increases protein synthesis leading to cell death. Nat Cell Biol 15, 481–490.

Harris CA, Haas JT, Streeper RS, Stone SJ, Kumari M, Yang K, Han X, Brownell N, Gross RW, Zechner R, *et al.* (2011). DGAT enzymes are required for triacylglycerol synthesis and lipid droplets in adipocytes. J Lipid Res 52, 657–667.

Hartman IZ, Liu P, Zehmer JK, Luby-Phelps K, Jo Y, Anderson RG, DeBose-Boyd RA (2010). Sterol-induced dislocation of 3-hydroxy-3-methylglutaryl coenzyme A reductase from endoplasmic reticulum membranes into the cytosol through a subcellular compartment resembling lipid droplets. J Biol Chem 285, 19288–19298.

Hashemi HF, Goodman JM (2015). The life cycle of lipid droplets. Curr Opin Cell Biol 33, 119–124.

Herker E, Harris C, Hernandez C, Carpentier A, Kaehlcke K, Rosenberg AR, Farese RV, Ott M (2010). Efficient hepatitis C virus particle formation requires diacylglycerol acyltransferase-1. Nat Med 16, 1295–1298.

Hetz C (2012). The unfolded protein response: controlling cell fate decisions under ER stress and beyond. Nat Rev Mol Cell Biol 13, 89–102.
Hetz C, Chevet E, Harding HP (2013). Targeting the unfolded protein response in disease. Nat Rev Drug Discov 12, 703–719.
Hiramatsu N, Chiang WC, Kurt TD, Sigurdson CJ, Lin JH (2015). Multiple mechanisms of unfolded protein response-induced cell death. Am J Pathol 185, 1800–1808.
Hodges BD, Wu CC (2010). Proteomic insights into an expanded cellular role for cytoplasmic lipid droplets. J Lipid Res 51, 262–273.
Hosokawa N, Wada I, Nagasawa K, Moriyama T, Okawa K, Nagata K (2008). Human XTP3-B forms an endoplasmic reticulum quality control scaffold with the HRD1-SEL1L ubiquitin ligase complex and BiP. J Biol Chem 283, 20914–20924.
Igal RA, Wang P, Coleman RA (1997). Triacsin C blocks de novo synthesis of glycerolipids and cholesterol esters but not recycling of fatty acid into phospholipid: evidence for functionally separate pools of acyl-CoA. Biochem J 324, 529–534.
Jo Y, Hartman IZ, DeBose-Boyd RA (2013). Ancient ubiquitous protein-1 mediates sterol-induced ubiquitination of 3-hydroxy-3-methylglutaryl CoA reductase in lipid droplet-associated endoplasmic reticulum membranes. Mol Biol Cell 24, 169–183.
Jonikas MC, Collins SR, Denic V, Oh E, Quan EM, Schmid V, Weibezahn J, Schwappach B, Walter P, Weissman JS, *et al.* (2009). Comprehensive characterization of genes required for protein folding in the endoplasmic reticulum. Science 323, 1693–1697.
Kassan A, Herms A, Fernández-Vidal A, Bosch M, Schieber NL, Reddy BJ, Fajardo A, Gelabert-Baldrich M, Tebar F, Enrich C, *et al.* (2013). Acyl-CoA synthetase 3 promotes lipid droplet biogenesis in ER microdomains. J Cell Biol 203, 985–1001.
Klemm EJ, Spooner E, Ploegh HL (2011). Dual role of ancient ubiquitous protein 1 (AUP1) in lipid droplet accumulation and endoplasmic reticulum (ER) protein quality control. J Biol Chem 286, 37602–37614.
Kurat CF, Wolinski H, Petschnigg J, Kaluarachchi S, Andrews B, Natter K, Kohlwein SD (2009). Cdk1/Cdc28-dependent activation of the major triacylglycerol lipase Tgl4 in yeast links lipolysis to cell-cycle progression. Mol Cell 33, 53–63.
Lakkaraju AK, Abrami L, Lemmin T, Blaskovic S, Kunz B, Kihara A, Dal Peraro M, van der Goot FG (2012). Palmitoylated calnexin is a key component of the ribosome-translocon complex. EMBO J 31, 1823–1835.
Li Z, Agellon LB, Allen TM, Umeda M, Jewell L, Mason A, Vance DE (2006). The ratio of phosphatidylcholine to phosphatidylethanolamine influences membrane integrity and steatohepatitis. Cell Metab 3, 321–331.
Lilley BN, Ploegh HL (2004). A membrane protein required for dislocation of misfolded proteins from the ER. Nature 429, 834–840.
Lin JH, Li H, Yasumura D, Cohen HR, Zhang C, Panning B, Shokat KM, Lavail MM, Walter P (2007). IRE1 signaling affects cell fate during the unfolded protein response. Science 318, 944–949.
Lin JH, Li H, Zhang Y, Ron D, Walter P (2009). Divergent effects of PERK and IRE1 signaling on cell viability. PLoS One 4, e4170.
Listenberger LL, Han X, Lewis SE, Cases S, Farese RV, Ory DS, Schaffer JE (2003). Triglyceride accumulation protects against fatty acid-induced lipotoxicity. Proc Natl Acad Sci USA 100, 3077–3082.
Liu P, Ying Y, Zhao Y, Mundy DI, Zhu M, Anderson RG (2004). Chinese hamster ovary K2 cell lipid droplets appear to be metabolic organelles involved in membrane traffic. J Biol Chem 279, 3787–3792.
Lu M, Lawrence DA, Marsters S, Acosta-Alvear D, Kimmig P, Mendez AS, Paton AW, Paton JC, Walter P, Ashkenazi A (2014). Opposing unfolded-protein-response signals converge on death receptor 5 to control apoptosis. Science 345, 98–101.
Lynes EM, Bui M, Yap MC, Benson MD, Schneider B, Ellgaard L, Berthiaume LG, Simmen T (2012). Palmitoylated TMX and calnexin target to the mitochondria-associated membrane. EMBO J 31, 457–470.
Lynes EM, Raturi A, Shenkman M, Ortiz Sandoval C, Yap MC, Wu J, Janowicz A, Myhill N, Benson MD, Campbell RE, *et al.* (2013). Palmitoylation is the switch that assigns calnexin to quality control or ER Ca2+ signaling. J Cell Sci 126, 3893–3903.
Masuda Y, Itabe H, Odaki M, Hama K, Fujimoto Y, Mori M, Sasabe N, Aoki J, Arai H, Takano T (2006). ADRP/adipophilin is degraded through the proteasome-dependent pathway during regression of lipid-storing cells. J Lipid Res 47, 87–98.
Meacham GC, Patterson C, Zhang W, Younger JM, Cyr DM (2001). The Hsc70 cochaperone CHIP targets immature CFTR for proteasomal degradation. Nat Cell Biol 3, 100–105.
Mehnert M, Sommer T, Jarosch E (2014). Der1 promotes movement of misfolded proteins through the endoplasmic reticulum membrane. Nat Cell Biol 16, 77–86.
Menendez JA, Lupu R (2007). Fatty acid synthase and the lipogenic phenotype in cancer pathogenesis. Nat Rev Cancer 7, 763–777.
Miyanari Y, Atsuzawa K, Usuda N, Watashi K, Hishiki T, Zayas M, Bartenschlager R, Wakita T, Hijikata M, Shimotohno K (2007). The lipid droplet is an important organelle for hepatitis C virus production. Nat Cell Biol 9, 1089–1097.
Moldavski O, Amen T, Levin-Zaidman S, Eisenstein M, Rogachev I, Brandis A, Kaganovich D, Schuldiner M (2015). Lipid droplets are essential for efficient clearance of cytosolic inclusion bodies. Dev Cell 33, 603–610.
Morito D, Hirao K, Oda Y, Hosokawa N, Tokunaga F, Cyr DM, Tanaka K, Iwai K, Nagata K (2008). Gp78 cooperates with RMA1 in endoplasmic reticulum-associated degradation of CFTRDeltaF508. Mol Biol Cell 19, 1328–1336.
Mueller B, Klemm EJ, Spooner E, Claessen JH, Ploegh HL (2008). SEL1L nucleates a protein complex required for dislocation of misfolded glycoproteins. Proc Natl Acad Sci USA 105, 12325–12330.
Mulvihill MM, Benjamin DI, Ji X, Le Scolan E, Louie SM, Shieh A, Green M, Narasimhalu T, Morris PJ, Luo K, *et al.* (2014). Metabolic profiling reveals PAFAH1B3 as a critical driver of breast cancer pathogenicity. Chem Biol 21, 831–840.
Nakatsukasa K, Kamura T (2016). Subcellular fractionation analysis of the extraction of ubiquitinated polytopic membrane substrate during ER-associated degradation. PLoS One 11, e0148327.
Novoa I, Zeng H, Harding HP, Ron D (2001). Feedback inhibition of the unfolded protein response by GADD34-mediated dephosphorylation of eIF2alpha. J Cell Biol 153, 1011–1022.
Ohsaki Y, Cheng J, Fujita A, Tokumoto T, Fujimoto T (2006). Cytoplasmic lipid droplets are sites of convergence of proteasomal and autophagic degradation of apolipoprotein B. Mol Biol Cell 17, 2674–2683.
Olzmann JA, Kopito RR (2011). Lipid droplet formation is dispensable for endoplasmic reticulum-associated degradation. J Biol Chem 286, 27872–27874.
Olzmann JA, Kopito RR, Christianson JC (2013a). The mammalian endoplasmic reticulum-associated degradation system. Cold Spring Harb Perspect Biol 5, a013185.
Olzmann JA, Richter CM, Kopito RR (2013b). Spatial regulation of UBXD8 and p97/VCP controls ATGL-mediated lipid droplet turnover. Proc Natl Acad Sci USA 110, 1345–1350.
Petschnigg J, Wolinski H, Kolb D, Zellnig G, Kurat CF, Natter K, Kohlwein SD (2009). Good fat, essential cellular requirements for triacylglycerol synthesis to maintain membrane homeostasis in yeast. J Biol Chem 284, 30981–30993.
Plemper RK, Böhmler S, Bordallo J, Sommer T, Wolf DH (1997). Mutant analysis links the translocon and BiP to retrograde protein transport for ER degradation. Nature 388, 891–895.
Ploegh HL (2007). A lipid-based model for the creation of an escape hatch from the endoplasmic reticulum. Nature 448, 435–438.
Pol A, Gross SP, Parton RG (2014). Review: biogenesis of the multifunctional lipid droplet: lipids, proteins, and sites. J Cell Biol 204, 635–646.
Rambold AS, Cohen S, Lippincott-Schwartz J (2015). Fatty acid trafficking in starved cells: regulation by lipid droplet lipolysis, autophagy, and mitochondrial fusion dynamics. Dev Cell 32, 678–692.
Satoh T, Chen Y, Hu D, Hanashima S, Yamamoto K, Yamaguchi Y (2010). Structural basis for oligosaccharide recognition of misfolded glycoproteins by OS-9 in ER-associated degradation. Mol Cell 40, 905–916.
Schneider CA, Rasband WS, Eliceiri KW (2012). NIH Image to ImageJ: 25 years of image analysis. Nat Methods 9, 671–675.
Scott DC, Schekman R (2008). Role of Sec 61p in the ER-associated degradation of short-lived transmembrane proteins. J Cell Biol 181, 1095–1105.
Spandl J, Lohmann D, Kuerschner L, Moessinger C, Thiele C (2011). Ancient ubiquitous protein 1 (AUP1) localizes to lipid droplets and binds the E2 ubiquitin conjugase G2 (Ube2g2) via its G2 binding region. J Biol Chem 286, 5599–5606.
Stein A, Ruggiano A, Carvalho P, Rapoport TA (2014). Key steps in ERAD of luminal ER proteins reconstituted with purified components. Cell 158, 1375–1388.
Stevenson J, Huang EY, Olzmann JA (2016). Endoplasmic reticulum-associated degradation and lipid homeostasis. Annu Rev Nutr 36, 511–542.
Stone SJ, Myers HM, Watkins SM, Brown BE, Feingold KR, Elias PM, Farese RV (2004). Lipopenia and skin barrier abnormalities in DGAT2-deficient mice. J Biol Chem 279, 11767–11776.
Suzuki M, Otsuka T, Ohsaki Y, Cheng J, Taniguchi T, Hashimoto H, Taniguchi H, Fujimoto T (2012). Derlin-1 and UBXD8 are engaged in dislocation and degradation of lipidated ApoB-100 at lipid droplets. Mol Biol Cell 23, 800–810.

Takahashi Y, Shinoda A, Kamada H, Shimizu M, Inoue J, Sato R (2016). Perilipin2 plays a positive role in adipocytes during lipolysis by escaping proteasomal degradation. Sci Rep 6, 20975.
Tamura T, Cormier JH, Hebert DN (2011). Characterization of early EDEM1 protein maturation events and their functional implications. J Biol Chem 286, 24906–24915.
Tang T, Abbott MJ, Ahmadian M, Lopes AB, Wang Y, Sul HS (2013). Desnutrin/ATGL activates PPARδ to promote mitochondrial function for insulin secretion in islet β cells. Cell Metab 18, 883–895.
Tang W (2004). Links between CD147 function, glycosylation, and caveolin-1. Mol Biol Cell 15, 4043–4050.
Taxis C, Vogel F, Wolf DH (2002). ER-golgi traffic is a prerequisite for efficient ER degradation. Mol Biol Cell 13, 1806–1818.
Thibault G, Shui G, Kim W, McAlister GC, Ismail N, Gygi SP, Wenk MR, Ng DT (2012). The membrane stress response buffers lethal effects of lipid disequilibrium by reprogramming the protein homeostasis network. Mol Cell 48, 16–27.
Tomoda H, Igarashi K, Omura S (1987). Inhibition of acyi-CoA synthetase by triacsins. Biochim Biophys Acta 921, 595–598.
Tyler RE, Pearce MM, Shaler TA, Olzmann JA, Greenblatt EJ, Kopito RR (2012). Unassembled CD147 is an endogenous endoplasmic reticulum-associated degradation substrate. Mol Biol Cell 23, 4668–4678.
Urano F, Wang X, Bertolotti A, Zhang Y, Chung P, Harding HP, Ron D (2000). Coupling of stress in the ER to activation of JNK protein kinases by transmembrane protein kinase IRE1. Science 287, 664–666.
Vashist S, Kim W, Belden WJ, Spear ED, Barlowe C, Ng DT (2001). Distinct retrieval and retention mechanisms are required for the quality control of endoplasmic reticulum protein folding. J Cell Biol 155, 355–368.
Velázquez AP, Tatsuta T, Ghillebert R, Drescher I, Graef M (2016). Lipid droplet-mediated ER homeostasis regulates autophagy and cell survival during starvation. J Cell Biol 212, 621–631.
Vevea JD, Garcia EJ, Chan RB, Zhou B, Schultz M, Di Paolo G, McCaffery JM, Pon LA (2015). Role for lipid droplet biogenesis and microlipophagy in adaptation to lipid imbalance in yeast. Dev Cell 35, 584–599.
Volmer R, Ron D (2015). Lipid-dependent regulation of the unfolded protein response. Curr Opin Cell Biol 33, 67–73.
Volmer R, van der Ploeg K, Ron D (2013). Membrane lipid saturation activates endoplasmic reticulum unfolded protein response transducers through their transmembrane domains. Proc Natl Acad Sci USA 110, 4628–4633.
Walter P, Ron D (2011). The unfolded protein response: from stress pathway to homeostatic regulation. Science 334, 1081–1086.
Walther TC, Farese RV (2012). Lipid droplets and cellular lipid metabolism. Annu Rev Biochem 81, 687–714.
Wang M, Kaufman RJ (2016). Protein misfolding in the endoplasmic reticulum as a conduit to human disease. Nature 529, 326–335.
Wang XZ, Harding HP, Zhang Y, Jolicoeur EM, Kuroda M, Ron D (1998). Cloning of mammalian Ire1 reveals diversity in the ER stress responses. EMBO J 17, 5708–5717.
Xu C, Ng DT (2015). Glycosylation-directed quality control of protein folding. Nat Rev Mol Cell Biol 16, 742–752.
Xu G, Sztalryd C, Lu X, Tansey JT, Gan J, Dorward H, Kimmel AR, Londos C (2005). Post-translational regulation of adipose differentiation-related protein by the ubiquitin/proteasome pathway. J Biol Chem 280, 42841–42847.
Ye Y, Shibata Y, Yun C, Ron D, Rapoport TA (2004). A membrane protein complex mediates retro-translocation from the ER lumen into the cytosol. Nature 429, 841–847.
Yen CL, Stone SJ, Koliwad S, Harris C, Farese RV (2008). Thematic review series: glycerolipids. DGAT enzymes and triacylglycerol biosynthesis. J Lipid Res 49, 2283–2301.
Younger JM, Chen L, Ren HY, Rosser MF, Turnbull EL, Fan CY, Patterson C, Cyr DM (2006). Sequential quality-control checkpoints triage misfolded cystic fibrosis transmembrane conductance regulator. Cell 126, 571–582.
Zehmer JK, Bartz R, Bisel B, Liu P, Seemann J, Anderson RG (2009). Targeting sequences of UBXD8 and AAM-B reveal that the ER has a direct role in the emergence and regression of lipid droplets. J Cell Sci 122, 3694–3702.